

Solar Powered Electric Vehicle

Brandon Kretchmer

Ryan Monahan

Aldo Garcia

Eric Garner

Brian Sims

Nnadozie Njoku

Michael Lahey

Nicolau Monteiro

Academic Advisor: Hansung Kim

Department of Mechanical and Civil Engineering
College of Engineering and Sciences
Purdue University Northwest
April 26, 2017

Executive Summary

The overall objective of the project is to design and fabricate an efficient solar powered electric vehicle. The objective of the project thus far was to produce a detailed first iteration design with planning materials. The vehicle is to adhere to the engineering guidelines stated for the Shell Eco-Marathon Urban Division competition. This competition is based on the overall efficiency of the vehicle over a six-mile course. This type of vehicle would be suited to replace traditional combustion engines for everyday transport activities. The use of solar energy to power the vehicle allows for more applicability, and a means of using green energy. The normalization of a vehicle of this type would dramatically reduce the amount of carbon dioxide produced by vehicles and reduce the demand for oil.

To accomplish this goal. Computer aided design software (CAD) and supporting software were used to plan, model, simulate, and analyze the various subsystems of the vehicle. The two engineering categories the vehicle subsystems fall into are mechanical or electrical.

The best designs were selected based on the following criteria: cost, design flexibility, manufacturability, assembly purposes, and overall safety. The best selected designs for the subsystems were modeled. The models were then integrated into the entire system to check for clearance issues during assembly. Some subsystems were simulated and analyzed thoroughly were purchased or fabricated. These subsystems include the frame and drivetrain. Hands on assistance was provided to create the previously mentioned subsystems. Other subsystems require more simulation and analysis to verify safety. Once completed, fabrication of the remaining subsystems may continue as planned.

Progression of the project will be primarily in optimization and fabrication of the current designs. Other design configurations should be explored to improve vehicle efficiency and safety. Components that were purchased and/or fabricated were designed to be flexible to allow for modifications that may be needed in the future. The first iteration design should be used as a starting point for future teams to make changes to what will someday be a Shell Eco-marathon competition vehicle.

Abstract

The overall objective of the project is to design and fabricate a solar powered electric vehicle. The objective of the project thus far was to produce a detailed first iteration design with planning materials. The vehicle is to adhere to the engineering guidelines stated for the Shell Eco-Marathon Urban Division competition. The competition does not require the use of a solar module, but this project will incorporate the use of solar energy to charge the vehicle battery. This competition is based on efficiency; therefore, energy efficiency will be of higher priority. Other major constraints on the project were the time and budget. To accomplish this goal, subsystems such as the frame, drivetrain, power, suspension, and steering, were designed individually and integrated into a master assembly model. SolidWorks, a computer aided design (CAD), software was used for design and modeling, as well as finite element analysis (FEA). Secondary support software such as Excel, Vsusp, and solar analyzing software were used to assist in the planning of the various subsystems as well as data collection and assortment. Subsystems that were modeled and analyzed through quantitative methods were purchased and fabricated. Subsystems that did not complete the design and analysis phase were not constructed. Further analysis is required to move these subsystems forward. In the future, optimization and new subsystem configurations should be prioritized. This project concluded with the first iteration of what will someday be a Shell Eco-marathon competition vehicle.

Keywords: CAD, Competition vehicle, Design, Engineering, Electric Vehicle, FEA, Solar, Solar Energy, Shell Eco-marathon, Vehicle Subsystem

Table of Contents

Introduction	1
Background	2
Objectives.....	3
Constraints	4
Environmental Impact	6
Approach	7
Frame/Chassis	7
Fabrication of Frame.....	11
Powertrain	14
Solar Panel	15
Battery Selection Options	17
Motor Sizing and Selection.....	19
Control Logic	24
Steering and Suspension	29
Steering Ratio	31
Results	35
Frame	35
Fabrication of Frame	39
Powertrain	40
Solar Panel	41
Battery.....	43
Motor and Control	45
Powertrain Mounting	46
Suspension and Steering	48
Wheel Alignment Specifications	48
Determining Optimal Geometry	49
Spring Rate and Effective Wheel Radius	50
Fabrication of Steering Components.....	52
Conclusions	56
References	58
Appendix A: Previously Retrieved Components.....	60
Appendix B: Solar Vehicle Stock Information.....	62
Appendix C: Frame Design.....	67
Appendix D: Bill of Materials	69
Appendix E: Frame Fabrication Drawings By Setup	70
Appendix F: Solar Panel Data and Graphs.....	79
Appendix G: Motor Sizing Calculations and Data	81

List of Figures

Figure 1. Example of Spaceframe.....	7
Figure 2. Go Kart with Chassis Designed to be Flexible.....	8
Figure 3. Theory Model to Exemplify Torsional Rigidity Parameter [6].....	9
Figure 4. Theory Model Applied to the Solar Car Chassis.....	9
Figure 5. Roll Bar Simplified Model.....	10
Figure 6. Frame Fabrication Process.....	11
Figure 7. Individual Drawing Example.....	12
Figure 8. Etching Section in Table Setup #1.....	13
Figure 9. Overall Powertrain Process.....	14
Figure 10. Powertrain Calculations Process.....	14
Figure 11. Powertrain Component Selection & Inclusion Process.....	15
Figure 12. Lithium Ion Battery Type Comparison.....	18
Figure 13. Motor Part-Load Efficiency (as a Function of % Full-Load Efficiency) [11].	19
Figure 14. Vehicle Free Body Diagram [12].	20
Figure 15. Power vs. Speed (Level Ground with no Acceleration).	22
Figure 16. Major Components of an Electric Vehicle [18].	24
Figure 17. Control Scheme of an EV Vehicle Driven by an Induction Motor with Vector Control [18].	25
Figure 18. Controlling Voltage and Speed [19].	26
Figure 19. Operation of an EV Controller [18].	27
Figure 20. Independent Rear Wheel Drive Control.....	28
Figure 21. Arduino Microcontroller.....	28
Figure 22. Arduino Breadboard with Potentiometer.....	29
Figure 23. Rack and Pinion System.....	31
Figure 24. Understeering vs. Oversteering.....	32
Figure 25. Ackerman Angle Depiction.....	33
Figure 26. Assembled Steering System.....	33
Figure 27. Final Chassis.....	35
Figure 28. Results for Tension in MPa Unit.....	35
Figure 29. Results for Tension in MPa Unit.....	36
Figure 30. Results for Angular Deflection in Degrees.....	36
Figure 31. Typical values for Torsional Rigidity [23].	37
Figure 32. Max Result for Tension in Y Direction.....	38
Figure 33. Max Result for Tension in X Direction.....	38
Figure 34. Max. Result for Tension in Z Direction.....	39
Figure 35. Belt Selection Chart.....	40
Figure 36. Powertrain 3D Model View #1.....	41
Figure 37. Powertrain 3D Model View #2.....	41
Figure 38. Solar Panel IV and IP Curves.....	42
Figure 39. Custom LiFePO ₄ Battery with BMS.....	44
Figure 40. Custom LiFePO ₄ Battery Charger.....	44
Figure 41. Custom Enclosure for Battery.....	45
Figure 42. Morningstar TS-45 Charge Controller.....	45
Figure 43. Motor Mount Design 1.....	46
Figure 44. Motor Mount Design 2.....	47

Figure 45. Motor Mount Final Design.....	47
Figure 46. Bearing Risers.	48
Figure 47. Wheel Alignment Parameters [25].	48
Figure 48. Input Parameters [26].	50
Figure 49. Input Parameters, Spring Rate [27].	51
Figure 50. MakerBot Replicator.	52
Figure 51. 3D Printed Steering Knuckle.....	53
Figure 52. Cut Location of Steering Column.....	53
Figure 53. Plating for Steering Column Mounting.	53
Figure 54. Steering Column Bushing.....	54
Figure 55. Front Suspension and Steering Subassembly.	54
Figure 56. Rear Lower Suspension Plate.....	55
Figure 57. Orthogonal Assembly View 1.	57
Figure 58. Orthogonal Assembly View 2.	57

List of Tables

Table 1. Solar Panel Test Data.	42
Table 2. Spring Rate Input Parameters.	50
Table 3. Spring Rate Results.	51

Introduction

Currently, one of the greatest engineering issues to tackle is the need for clean energy sources. Much of the world is highly dependent on natural gases and coal to produce electricity. Although this power source is abundant, it is shown to assist in global warming. Furthermore, extraction methods such as fracking are shown to have detrimental effect on the environment, namely earthquakes.

One source of energy being heavily studied is solar energy. Until recently, the efficiency of the solar panels, used in collection of solar energy, was too low for it to be a viable option for replacing energy obtained from fossil fuels. Advances in materials has paved the way for using solar energy as a renewable resource that is slowly meeting the energy demands that society has become accustomed to.

According to the EPA, transportation accounted for 26% of the total Greenhouse Gas emissions in the year 2014 [1]. For this project, the concept of a solar vehicle will be designed and fabricated. Vehicles have already been modified to run on alternative sources for fuel, so for this project, an urban application solar car will be designed under specifications for the Shell Eco-marathon Urban Concept Battery Electric competition.

The project is focused on the design of an electric driven vehicle that can regenerate power using solar energy technology. If this type of vehicle became a standard commercial vehicle, the demand for fuel would decrease substantially. Designing this vehicle for practicality is the primary difficulty. The vehicle must be lightweight to minimize the size of the motor required to withstand urban transport needs. The vehicle is being designed to house one driver; practically, there would be need for additional space for other passengers and materials. Another consideration in the use of solar energy to power a vehicle is that the solar panel must be efficient enough to generate enough power for propulsion in a reasonable amount of time. This leads to a variety of decisions that must be considered during the design process.

Both mechanical and electrical engineering considerations must be taken into account for the project. Components must be suitable for the application of the urban concept division of the Shell Eco-marathon. Components will be purchased and manufactured from raw materials to suit the application. Some components will need to be machined to specifications due to the abnormal size of the vehicle. Decisions will be made based on monetary constraints and fabrication feasibility.

Background

The solar car project was initially started in the fall of 2015. The goal of that year's team was the same as the current team's, with the Shell Eco-marathon guidelines remaining the same. A finite number of components were obtained or purchased, and connections were made with a fabrication shop nearby for welding of the frame. The list of parts obtained by the previous group is as follows:

- 9x 24' Length 1" Square Aluminum 6061 Tubing
- 1 (sealed) rack and pinion
- 2x tie rod ends
- 2x sleeves
- 2x angle adapter
- 1 steering wheel
- 1 solar panel
- 1 steering column with hardware
- 1 master cylinder
- 1 brake pedal assembly
- 4 wheels
- 1 (4') brake line

The previous team also devised a suspension response simulation, and various simulations of their designed frame. Since the frame was redesigned and a new suspension setup was augmented, these materials will no longer have any relevancy. Acquired materials will be implemented into the new design.

Pictures of the previously acquired components can be viewed in Appendix A.

Objectives

The long-term objective of this project is to design, fabricate and assemble a fully functioning vehicle powered by solar energy, which in the future can be used to compete in the Shell Eco-Marathon. The race car competition is sponsored by Shell and takes place in Detroit, MI. The goal for this year's team is to develop a complete set of plans, design solar car's concept, and to purchase critical components within our budgetary constraints. This will consist of the following:

- Frame
 - Frame design, analysis, and fabrication
- Powertrain
 - Powertrain design
 - Motor research, selection and purchase
 - Parametric analysis of required power
 - Control research, design, and purchase
- Battery research, selection, and purchase
 - Management of battery life and safety
 - Solar energy charging capability
- Steering and Suspension
 - Design Steering system meeting Shell Eco-Marathon requirements
 - Design Steering system mounts
 - Design Suspension system
 - Design Suspension system mounts

Finalization of design plans and purchase of components within the budget are to be completed by May 2017.

Constraints

Since the vehicle is to be used in the Shell Eco-marathon competition, engineering standards are written in the rulebook for the urban concept division [2]. With the goal of designing an energy efficient vehicle, matters such as safety, connections for equipment, size limits, visibility are all considered. If these constraints are not met, the vehicle will not be permitted in the Shell Eco-marathon race in the future.

Spatial constraints were of primary concern during the design phase. Since material was purchased by previous teams, frame design and fabrication were started before the complete model was finished; therefore, when designing the various systems of the vehicle, the designer would need to check the frame model to assure that interference with the frame was not occurring. This added one more factor to consider during the design process.

Budgetary constraints were a major problem for the team. Since the team acquired \$3,000 in grants, the team was able to purchase key components such as the motor, battery, frame material, powertrain, and suspension components. The team used the budget below to allocate funds; it is important to note that these values are projected costs and the actual budget can be found in Appendix B:

- Motor – 4hp Motor from Allcart (\$1400.00)
- Battery – Lithium Ion (\$780.00)
- Powertrain Components – McMaster Fabricated Components (\$150-\$250)
- Suspension Components – Raw Materials, Machining, and Shocks (\$800-\$900)
- Mounting Materials – Aluminum Plating (\$500.00)

Unfortunately, since many of the components are more expensive, cheaper options had to be explored. These cheaper alternatives are less reliable, and lead to issues purchasing components through school grant means. If the budget was not so tight, this would have proved to be less of a problem. Even though cheaper options allowed for more budgetary flexibility, the total expected cost of all the materials for complete vehicle assembly will easily peak over \$4000. This means that not all materials will be able to be purchased this year.

Access to the manufacturing lab is limited to engineering students, so fabrication constraints were present throughout the project. The team needed to send out raw material to be fabricated. To minimize this fabrication time constraint, the team attempted to purchase finished components whenever possible. Limitations were also set to minimize the number of custom components as well. Some components could not be easily purchased; however, sending the components out to be fabricated ultimately took a tremendous amount of time. Since the weld shop was completing this project voluntarily, the frame fabrication took much longer than expected.

If this project was commercialized to replace conventional combustion engines, the results would directly affect individuals and companies. Individuals would be given more options when purchasing vehicles. Companies could make various types of vehicles to suit the demands of customers. This is already occurring in hybrid vehicles and electric vehicles. Electric drive

vehicles are already in existence, but these vehicles are not very spacious and require outlets to recharge constantly. The need for constant recharge would be eliminated harnessing solar power to energize the battery. The production of electric motor drive vehicles that are capable of performing similarly to combustion engines will lead to a revolution in passenger vehicles.

Currently there are no political or societal constraints with respect to electric motor vehicles. Legal constraints for electric vehicles are different in various states. The most common being a minimum speed requirement to use the road. In an effort to minimize the amount of greenhouse gases, 40 of 50 states currently provide tax benefits for owning and using Hybrid Electric Vehicles (HEV).

Environmental Impact

Creation of feasible alternative energy vehicles will have a positive impact on the environment. Since combustion engines never achieve complete combustion, resulting extraneous gases add to the problem of global warming. Electric motors produce zero emissions; therefore, the application of urban electric driven vehicle will dramatically decrease the amount carbon dioxide (CO₂) contributing to global warming. One other environmental factor should be considered when weighing the switch from combustion engines to electric motors.

Electric motor drives require a power source. Due to the need to apply many life cycles to the battery and the need for lightweight application, the use of lithium ion batteries are inevitable. Lithium is a rare-Earth element which produces considerable waste water to obtain. This would result in a negative impact on the environment. Regulations should be in place to minimize the amount of waste water for lithium harvesting.

Approach

Any design project will require the use of many different types of software and research to achieve the objectives. SolidWorks will be used for the modeling, drafting, and assembling of all the components. Research on electrical components for performance and purchasing will use journals and web sites. Engineering Equation Solver (EES) and Microsoft Excel was used to perform a parametric analysis to determine the appropriate size of the motor and other various safety factor analysis. Suspension and steering parameters were determined using Vsusp, an online available software.

Frame/Chassis

The chassis is defined as the basic structure of any vehicle. It is the central piece to which all other components are attached. Apart from structural integrity, this elementary part of the vehicle will protect the driver in case of an accident; it plays a big role in the car's safety. As the solar car is aimed to participate in an efficiency competition, it was necessary to design a chassis as light as possible, while maintaining a high standard of safety.

The first step in designing the chassis was to comprehend all the competition rules about the chassis. The rules concerning the chassis are basic, which provide a certain freedom in design. However, more constraints were added along the manufacturing process, which was conducted by a local welding company. For example, the company requested that a small gap be left between each connecting member to have some space for the welding procedures. Therefore, once all the constraints were known, it was necessary to determine the type of our chassis. We decided to have a spaceframe chassis. This type of chassis is constructed from an arrangement of small simple members which derive a larger frame (Fig. 1).



Figure 1. Example of Spaceframe.

A spaceframe chassis is very much like a truss structure, which is a combination of small members in a triangular arrangement that is in either tension or compression. This of course is in an ideal situation. This characteristic assures the members have zero minimal bending moments, allowing the frame to be designed with small sized cross-section members [3]. This would result in a lighter frame that would increase the car's efficiency. Newton's Second Law states that:

$$\text{Force} = \text{Mass} \times \text{Acceleration}$$

Given an equal force, a lighter solar car will accelerate quicker at all conditions. With a quicker acceleration, the solar car will reach a higher speed faster and help meet the performance demanded by the Shell Eco-marathon. Also, the spaceframe is cheaper in comparison to other types of chassis, and easy to build and modify. With this type of frame in mind, it was time to decide on what material to use. Since the previous team made a purchase of Aluminum 6061 as raw material, the decision to utilize this material was made. Aluminum 6061 was a favorable choice, providing a light frame stiff enough to support multiple driving loads.

Designing an automotive chassis depends primarily on the comprehension of different types of loads that act on it. While in use, automotive chassis endure several loads that can be defined globally (overall deformation of the chassis) as listed below [4]:

- Longitudinal Torsion
- Vertical Bending
- Lateral Bending
- Lozenge Horizontal

For detailed description of the loads listed above, refer to Appendix C.

Multiple types of loads acting on a car will directly influence the vehicle's behavior; therefore, if the vehicle is not rigid enough, it will have resulting effects on direction control, as well as in the passenger's protection and comfort. Lack of rigidity will make the vehicle less sensitive to the driver's actions. In other words, it will be hard to determine the vehicle comportment with the road. However, the absence of enough rigidity is not always a problem. Go Karts are an exception as they have no suspension, and the frame must act like a suspension system (Fig. 2). Accordingly, it is essential to know chassis' rigidity, specifically torsional rigidity. When a vehicle has a satisfactory torsional rigidity, which is the resistance to longitudinal torsion loads, it also has a satisfactory resistance to remaining global loads. Therefore, the analysis of torsional rigidity is a determinant for an optimal chassis [5].



Figure 2. Go Kart with Chassis Designed to be Flexible.

With the intention of advancing quickly in through the design and using the material already purchased by the previous senior design team, the modeling process of the spaceframe was

completed mainly through trial and error. Team members decided based on several designs, which were examined considering a variety of factors. To ensure the final design was optimal, finite element analysis (FEA) was performed to study the torsional rigidity of the car. The software used for this analysis was the SolidWorks finite element package.

The theoretical model to study longitudinal torsion consists of a square tube in which one extremity is fixed and the other is applied a torque with relation to the longitudinal axis (Fig. 3) [6].

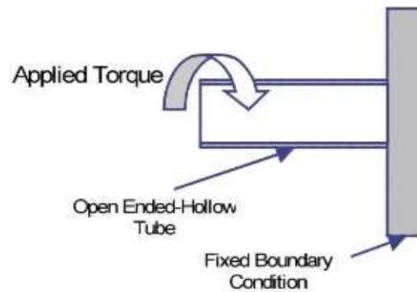


Figure 3. Theory Model to Exemplify Torsional Rigidity Parameter [6].

In this model, the tube represents the chassis and its extremities, the rear and front suspension. This model can be applied to the solar car chassis using FEA (Fig. 4).

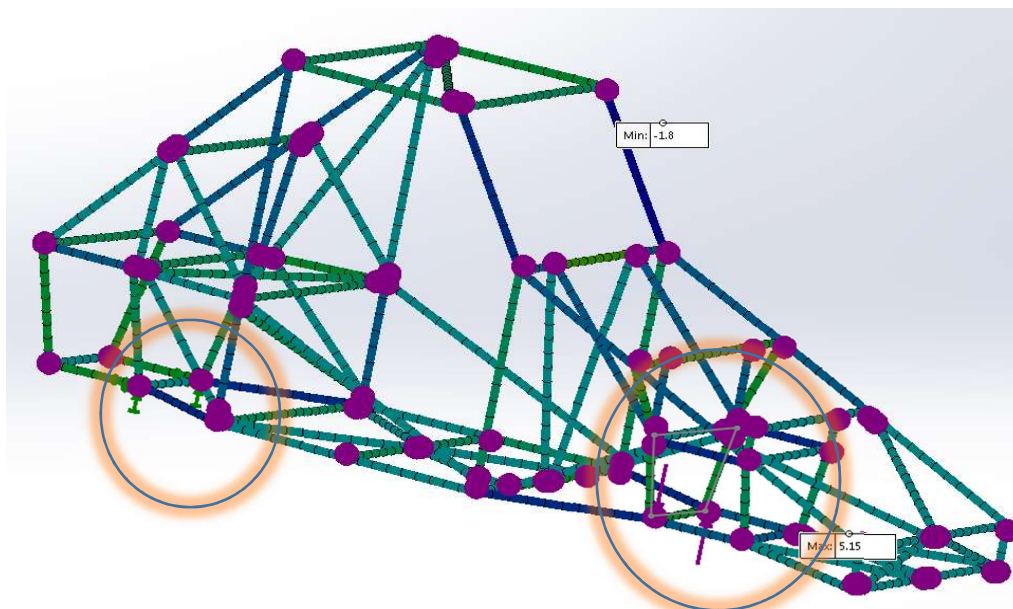


Figure 4. Theory Model Applied to the Solar Car Chassis.

Torsional rigidity can be evaluated by dividing the torque applied on the chassis by the angular deflection. The mathematical representation is as follows:

$$K_t = \frac{T}{\theta}$$

Where,

- K_t - Torsional rigidity
- T - Applied torque
- θ - Angular deflection

The finite element method simulation was performed in accordance to the following guidelines:

- The model was constrained by applying a geometry fixture on the rear suspension
- A 1000N force was applied in the opposite direction along the vertical plane in each node of the front suspension. This creates a twist about the frame.

Torsional rigidity of the frame was just one of the factors to be considered in designing the frame. One of the rules of the Shell Eco-marathon is that the car must withstand a force of 700N applied in all three directions at the roll bar. This can be illustrated with the roll bar considered as a beam with both ends fixed and a vertical force being applied (Fig. 5).

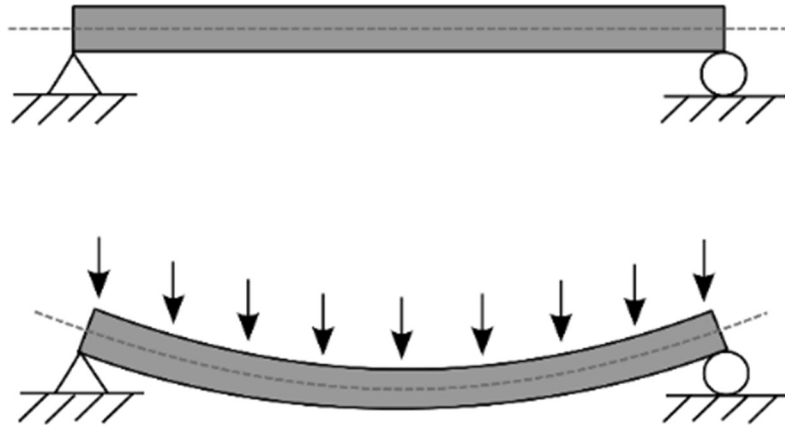
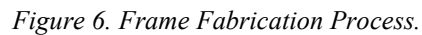


Figure 5. Roll Bar Simplified Model.

The roll bar analysis was performed using the same software used for torsional rigidity. The FEA static simulation was performed in accordance with the following guidelines:

- Both the rear and front suspension were fully fixed
- A 700N force was applied to the roll bar in all three directions (one in each simulation)

Not only was the team responsible for the design of the frame, but also for the manufacturing of the frame. The team worked in conjunction with Arrow Pin and Product Inc. in Chicago Heights, Illinois. Through this process, the team gained experiential learning through manual labor and drafting opportunities. The team followed a specific process to fabricate the frame (Fig. 6).



11

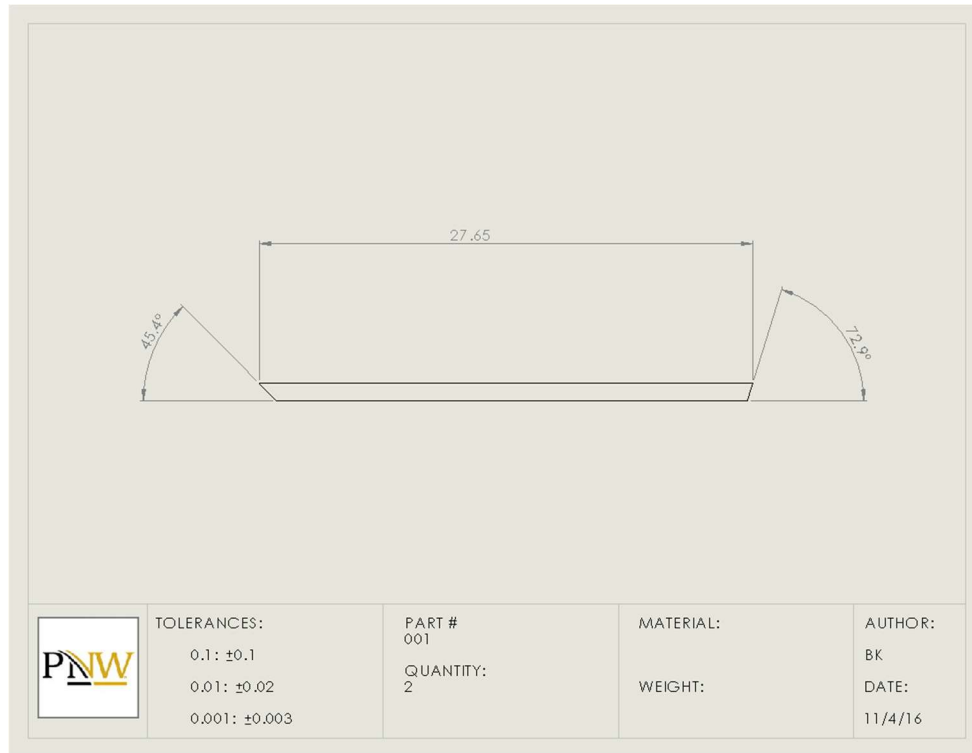


Figure 7. Individual Drawing Example.

Drafting materials were created using SolidWorks. To create the needed models, planar sections were removed from the overall frame model. Examples of some planar sections are as follows: Side Planar Surfaces, Individual Trapezoid Planar Surfaces, Bottom Section Planar Surfaces, and Rear Planar Surface. Assembly files were created to orientate the sections to make use of the overall platform. Various table setups were created to create as many planar sections were built against the welding platform as possible. This would effectively decrease the amount of time for frame fabrication. Creating the entire frame in this manner allowed for the frame construction to match as similar as possible to the modeled frame. Since this process may lead to slight variations in the final welding when the sections are oriented in 3D space, once the frame is completely built, the frame model may need to be modified slightly.

Using the assembly files, table setup drawings were created for the weld shop (Appendix E). Since the weld shop does not have 3D modeling software, there was great importance on making the drawings concise and clear. The table setup drawings include information such as dimensions, part numbers, and notes. There was a total of four table setups. The first three setups were all planar sections created against the table, and the fourth setup was combining all the created sections with the addition of the cross members.

The first step in the table preparation was the removal of rust and top level to create a flat surface. After creating the reference and center lines, the team used the table setup drawings to etch the member locations into the welding platform (Appendix E). Once the member locations are etched into the table, stops were tacked on the table to properly seat the members in their respective locations.

Raw material, 1" square aluminum tubing, was cut to specifications using the individual member drawings and BOM. Members were then located on the table and TIG welded together. Before welding, the surface of the locations to be welded was scrubbed to clean and remove oxidation. This process involved welding the joints, allowing the joints to cool, and inspecting the section to verify straightness. The welding process followed the four table setup drawings. Once sections were finished, they were stored until needed in the fourth table setup drawings. Sections were welded together in the fourth table setup (Fig. 8).



Figure 8. Etching Section in Table Setup #1.

The frame was then transported back to Purdue University Northwest and stored in the Anderson 164. Systems such as steering, suspension, and powertrain will then be sequentially mounted to the frame after being purchased or fabricated.

Powertrain

The powertrain of the vehicle will be defined by the system that transmits power from the motor to the wheels. A “V” belt drive system was chosen for the application due to strength and transmission efficiency. A belt drive system is also cost effective and will adhere to the spatial constraints set by the frame. A process was used to systematically select components for the powertrain (Fig. 9).

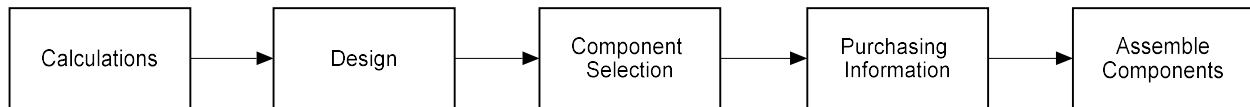


Figure 9. Overall Powertrain Process.

Calculations are required to verify the performance and the safety of the individual components. The individual components that have calculations associated are the belt, shaft, and bearings. Calculation inputs were desired performance, motor parameters, and frame spatial constraints (Fig. 10). Various types of analysis were used to determine component sizing and factor of safety.

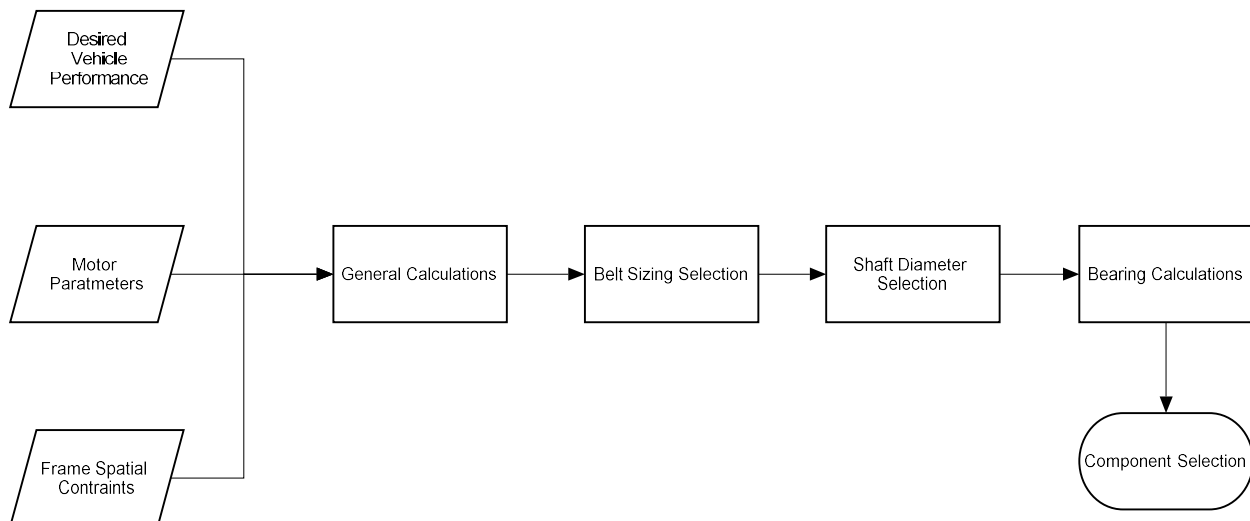


Figure 10. Powertrain Calculations Process.

General calculations were used to determine the gear ratio required for vehicle performance. Using the equation for calculating the arc length of a circle ($s = r\theta$), the arc length (s) the tire will travel through in one revolution can be calculated knowing the radius of the tire (r), and multiplying it by 2π . Multiplying the distance traveled per revolution by the max RPM's of the motor, yields the maximum distance traveled per unit time (velocity). Without gear reduction, the vehicle has the potential to travel in excess of 100 mph, which is a safety consideration, so the gear ratio was modified to adjust the top speed of the vehicle. The minimum gear ratio required was determined to be 2.4. This would have the vehicle top speed be approximately 40mph. To improve motor efficiency, the highest gear ratio feasible was chosen. A gear ratio of 2.6 allowed the top speed of the vehicle to be approximately 35mph. Knowing the gear ratio allows appropriate pitch diameters to be chosen.

Belt sizing is a function of horsepower, application, and belt speed. For vehicle operation, there is no steady state running speed. The speed will be determined by the driver and will vary with time. For simplicity and cost effectiveness, a V belt was chosen for the application. With the parameters determined, an appropriate “V” belt can be selected for the application. Information pertaining the “V” belt must be verified for powertrain use. These parameters include initial tension and minimum pulley sheave diameter. These parameters were varied through design and research.

The next step was to determine an appropriate size for the primary shaft. To determine the shaft size, the forces acting on the shaft must first be determined. Modified Goodman Theory criterion was then applied to the loading condition to determine the size of the shaft given a desired factor of safety. Bearings were selected based off manufactures data provided.

Components were chosen from the McMaster-Carr website. Due to time constraints, components were purchased so that no further machining would be required. Components chosen were then added to a purchase list and the overall SolidWorks model (Fig. 11). When the powertrain component arrived, assembly of the powertrain components were performed to create a drivetrain test stand.

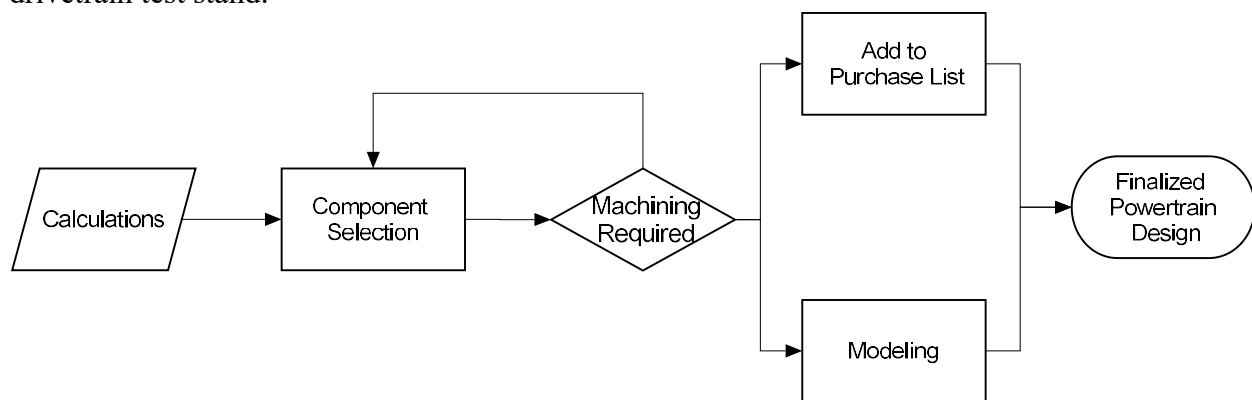


Figure 11. Powertrain Component Selection & Inclusion Process.

Solar Panel

There are several different forms of energy that are feasible options for use in today’s society. Although the main source of energy is obtained through the use of gas, oil, and the burning of coal, alternative forms of energy are being sought due to the inconveniency that gas and oil are nonrenewable sources of energy and negatively affect the environment. Some of these alternate sources include hydroelectric, wind, tidal wave, bioenergy, and solar energy. With these alternate forms of energy come respective advantages and disadvantages; the feasibility of each form has its own constraints. For example, it makes more sense to use wind turbines in vast, open areas with frequently occurring wind gusts as opposed to trying to place them in congested cities. Expanding on this point, it makes more sense to use solar panels in the Southwest region of the United States, where it is sunny, clear skies, and hot, rather than it does to use them in the Northeast. However, solar energy research is growing; with continuous technological advancements, the use of solar panels and solar cells will likely become a very prosperous, alternate form of renewable energy.

The first acknowledgment of solar energy dates back to 1839 when French physicist, Edmund Becquerel, discovered that some materials would produce an electric current when they were exposed to sunlight. From there, Albert Einstein won a Nobel Prize after his work with photovoltaic technology in 1905. The first photovoltaic module was built in 1954 by Bell Laboratories, but lacked widespread use because too little was still known about the capabilities of it. Moving forward to the 1960's, solar energy was used to generate power aboard a spacecraft, enhancing its reliability and feasibility of use. Finally, in the 1970's, during the energy crisis, solar energy was adapted for commercial use [7]. So how do photovoltaic, solar, cells actually work? "For solar cells, a thin semiconductor wafer is specially treated to form an electric field, positive on one side and negative on the other. When light energy strikes the solar cell, electrons are knocked loose from the atoms in the semiconductor material. If electrical conductors are attached to the positive and negative sides of the cell (forming an electrical circuit), the electrons can be captured in the form of an electric current" [7]. Combining several cells together is referred to as a module; combining several modules is known as an array. These arrays support common 12 volt electrical systems. Furthermore, treated photovoltaic arrays can be produced and distributed in the form of panels for personal use.

The solar panel being used is 1,440 square inches, or approximately 1 square meter, and is to be placed on the hood of the vehicle, exposed to direct sunlight. This solar panel was donated to the Solar Car Vehicle team by Purdue University Northwest's Professor, David Kozel, and the Electrical Engineering Department. In order to determine how the solar panel works and how efficient it is, certain tests and experiments were completed to find out the capabilities of the solar module. Seeing as how the panel has one positive and one negative electrical leads connected to the back of it the current can be measured. The voltage and current curves can be created by using a solar analyzer and its accompanying software to collect data. An AMPROBE Solar Analyzer was plugged into an electrical outlet for power and then be connected via a USB jack to any laptop or computer with downloadable software that collects solar data in terms of voltage and current. Furthermore, the solar analyzer will be connected to the positive and negative leads on the back of the panel. Certain variables such as irradiance, date, temperature, and solar cell area can be input to the analyzer to help make the results more accurate. Then, with the panel angled towards the sun, a scan can be completed using the analyzer to measure the voltage and current being generated by the photovoltaic process, as well as output the panel's overall efficiency. This process was completed several times to ensure that the measurements obtained are accurate. Seeing as how the sun's energy will differ from day-to-day, precision is not a desired goal to achieve when using the panel, but data acquired should not vary tremendously.

Battery Selection Options

One of the most important components in designing and implementation of the solar vehicle is the battery. The battery is required to power and propel the vehicle and must be able to be charged by the solar panel. This configuration must be safe for the driver operating the vehicle. These are three of the main factors to consider when choosing a battery. Two types of batteries meet these criteria: deep cycle lead acid and Lithium ion. While these factors were used to evaluate the decision on which type of battery to select, the most important qualifier was whether or not the battery was compatible with the motor selected for the car. The final decision for the battery was made based off of what type of motor was selected.

Deep Cycle Lead Acid

The first type of battery that was considered was the lead acid battery. Certain types of lead acid batteries are ideal for the application of a solar powered electric vehicle, however, not just any type of lead acid battery would be feasible. For example, the battery that is used to start an engine in most gasoline fueled cars would not be able to be used for this project. Starter batteries are only able to give off one quick burst of energy and then be recharged by the alternator while driving. The type of battery that has to be used for any electric vehicle is a deep cycle battery. Deep cycle batteries are specially built so that they can provide consistent power over longer periods of time. The most important aspect of a deep cycle battery is that they can be discharged from full capacity to depletion many times. While a traditional starter battery could be fully discharged approximately ten times before it loses its ability to hold a charge, a deep cycle battery can be fully discharged several hundred times before the same outcome is reached. Deep cycle lead acid batteries can be charged very simply with a solar panel; however, they do require a charging controller to ensure that the battery has a long life with high performance. The charging controller charges the battery in three stages to ensure this. The first stage is bulk charge. The battery is charged to 80% of its maximum capacity, voltage, and amps, then, stops when the voltage reaches approximately 14 volts. The second stage is absorption charge; the voltage continually increases until the battery is around 98%. The third and final stage is float charge; at low voltage and low amps, the battery is charged to 100% while not overcharging or boiling the acid [8]. Knowing that lead acid batteries are capable of powering the car, and that they can be charged by a solar panel, the selection of a deep cycle lead acid battery can be viewed as a feasible solution.

There are two types of deep cycle lead acid batteries that would be applicable for an electric vehicle: sealed and flooded batteries. Flooded batteries must be regularly serviced in order to maintain efficiency and battery life. The maintenance is done by filling the individual cells of the battery with distilled water to maintain an optimum specific gravity, which is measured by a hydrometer. To keep the battery running efficiently, the case must be taken off and this procedure must be done about once a month [8]. With a sealed battery this is not necessary, and as the name suggests, the battery is permanently sealed. A safety problem arises when considering a flooded battery; even if proper precautions are taken, any time exposed acid is involved, an accident is subject to higher probability. For that reason, using a flooded battery was out of the question. Even though sealed batteries are approximately twice as expensive as

flooded, safety is more important. With all of this information taken into account, it was determined that if a lead acid battery was to be used, it would be a deep cycle sealed battery.

Lithium Ion

The second type of battery that was considered for this project was a Lithium ion battery. Lithium ion batteries are ideal for solar powered electric vehicles. If money was not an obstacle, the battery selected would be Lithium ion. Most Lithium batteries, regardless of the cathode material, can be cycled well over one thousand times because Lithium has the largest electrochemical potential and specific energy, pound for pound, of any metal. Many Lithium ion battery chemistries were developed specifically to be charged by solar panels, only a simple controller is required to charge them. The rate of charge is determined solely by the solar panel that is being used. Another advantage to using Lithium ion is that they are extremely low maintenance, and only require a simple battery management system (BMS) to ensure safety and long battery life [9].

There are many types of Lithium ion batteries, so the first process in evaluating Lithium ion was deciding which type would be used. Overall, six types of Lithium ion batteries are in common usage: Cobalt Oxide (LCO), Nickel Cobalt Aluminum Oxide (NCA), Nickel Cobalt Manganese Oxide (NCM), Manganese Oxide (LMO), Titanate (LTO), and Iron Phosphate (LFP). Lithium ion batteries are named for the active materials, cathodes, that give the battery its unique characteristics. All of these different cathode materials offer different advantages to the battery. For example, Iron Phosphate gives the battery excellent thermal stability, while Cobalt Oxide has poor thermal stability. The first process was to eliminate those types of Lithium ion batteries that are not applicable for an electric vehicle. Lithium Cobalt Oxide is more applicable for laptop batteries, and Lithium Titanate/Lithium Nickel Cobalt Aluminum Oxide are much more powerful than what would be necessary for such a small application [10]. For the three types of batteries that remain, the parameters used to evaluate them were cost, performance, life span, and safety (Fig. 12).

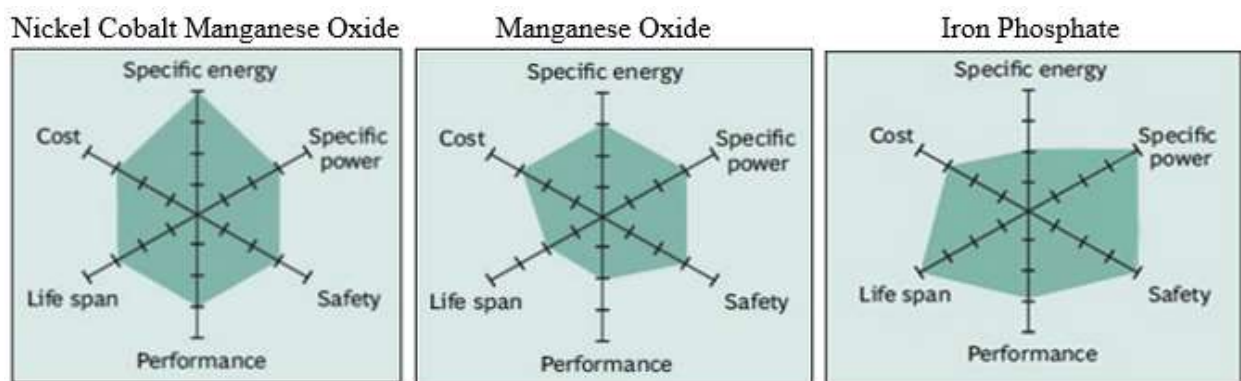


Figure 12. Lithium Ion Battery Type Comparison.

While examining the types of batteries, it was apparent that the cost and performance of the three were relatively similar, so instead, emphasis was put on life span and safety. Superiority was denoted as the Iron Phosphate battery, which is intuitive as it was first developed in an effort to replace lead acid batteries. It is by far the safest option since it was designed to be used at high

voltages for a long time; other batteries would falter in such conditions [10]. If the battery is used, and stored, properly it can be used for approximately 2000 cycles. This is much higher than Nickel Cobalt Manganese Oxide and Manganese Oxide. In addition to advantages that come with safety and life span, Iron Phosphate also has relatively high specific energy and excellent specific power. Specific energy is the amount of energy that the battery has per unit mass, and specific power is the amount of energy per unit volume. There are two important characteristics to mention: firstly, the vehicle has a weight limit, secondly, the area where the battery will be stored is relatively small. This will allow the vehicle to have maximum power while not weighing down the vehicle or taking up much room. After all the factors had been evaluated, it was clear that Lithium Iron Phosphate (LiFePO_4) was the best battery option if the vehicle was to run using a Lithium ion battery.

Motor Sizing and Selection

Since the Shell Eco-marathon competition is based on efficiency, appropriately sizing the motor correctly is critical. Oversizing or under sizing the motor can result in drastic reductions in efficiency and potentially lead to shorter life and higher maintenance costs.

Electric motors are usually designed to run from fifty percent to one hundred percent of rated full load. Motors that are either overloaded or run below 50% rated load see drastic decreases in efficiency (Fig. 13).

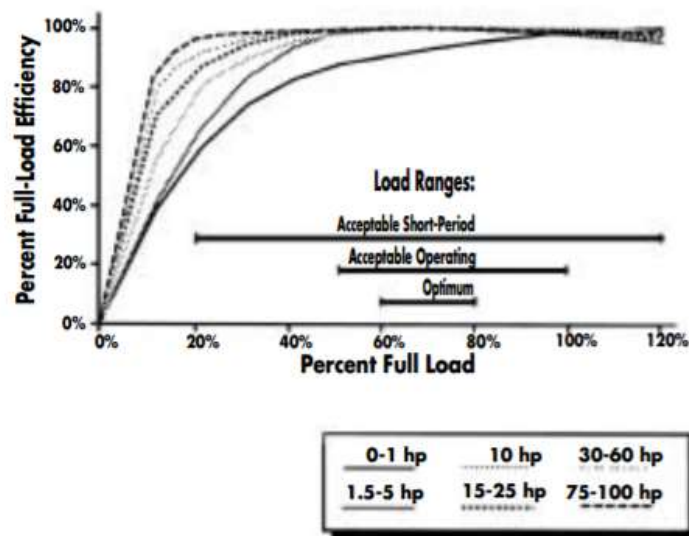


Figure 13. Motor Part-Load Efficiency (as a Function of % Full-Load Efficiency) [11].

Additionally, motors often achieve maximum efficiency when run around 75% of full load [11]. For these reasons, choosing a motor that will provide the proper power output is necessary for an efficient vehicle.

Mechanical power can be calculated using the motor torque and the revolutions per minute (RPM) of the output shaft.

$$\text{Power (hp)} = \text{Torque (ft-lbs)} \times \text{RPM} / 5252$$

To determine the proper size motor for the solar vehicle competition application, the power required from the motor can be determined by performing a parametric scenario study. The analysis can be performed by treating the vehicle as a free body diagram (Fig. 14). All the external forces being applied on the vehicle can be summed up to determine the total external force on the vehicle. The amount of power output from the motor that is needed to counteract the external forces can then be quantified. From the free body diagram, each of the individual forces can be calculated.

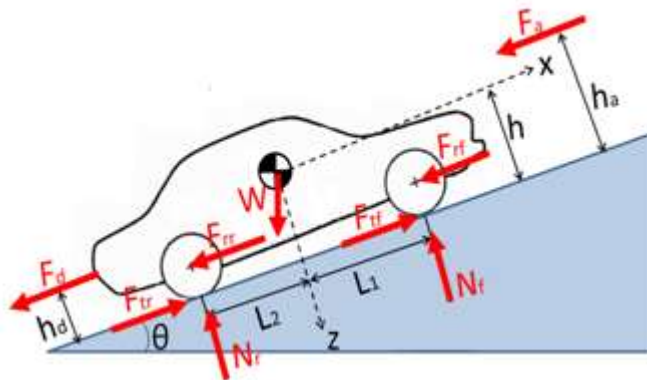


Figure 14. Vehicle Free Body Diagram [12].

The forces acting on the vehicle are as follows:

- **Rolling Resistance:** This force occurs due to the deformation of the tires. The tires will deform to create a bulge in the rubber tire. The deformation creates a moment in the opposite direction of the tire rotation. This creates resistance in the rolling of the tire. This resistance is a function of the weight of the vehicle, road conditions, and the angle of inclination. For the purpose of analysis, the standard coefficient for rolling resistance of 0.018 was used [13]. The higher the angle of inclination, the less the normal force acting on the tires. The lower the normal force acting on the tires, the less deformation in the tires.
- **Climbing Resistance:** This force is due to the change in elevation of the vehicle. If the vehicle is traveling on level ground, the climbing resistance would be zero. Climbing resistance is a function of weight and angle of inclination. Angle of inclination and climbing force are proportional. The higher the angle of inclination, the higher the climbing resistance exerted on the vehicle.
- **Acceleration Resistance:** Simply, this resistance is in accordance with Newton's 2nd Law. To accelerate a mass, a force is required; therefore, as the vehicle is accelerating, an external force is present on the vehicle. The acceleration resistance is a function of the weight of the vehicle, acceleration, and the inertial coefficient. The inertial coefficient is a function of the mass and quantity of rotating parts. Since the drive train of the electric vehicle will have minimal rotating parts, the inertial coefficient can be assumed to be approximately 1.06 [13].

- **Aerodynamic Drag Force:** The vehicle is moving through the air. Air is a gas and exhibits quality as such. As air passes over the vehicle, low pressure air pockets are created on the backside of the vehicle. This creates the phenomenon known as aerodynamic drag force. Aerodynamic drag force is a function of the density of air, frontal area, velocity, and drag coefficient. For analysis purposes, the density of air will be considered for standard atmospheric conditions and the frontal area of the vehicle will be considered to be the maximum frontal area as denoted by the Shell Eco-Marathon rules [14]. The coefficient of drag can be minimized during the design of the body of the vehicle. For analysis, it is assumed that this vehicle will have a smaller drag coefficient compared to a small vehicle. It will be assumed as 0.15. Although this assumption is not optimal, since the vehicle will be moving at a relatively low speed, the forces due to aerodynamic drag will be relatively small.

It should be denoted that for parameters that are yet to be determined such as: vehicle weight, frontal area, inertial coefficient, etc., that max extremes were used for calculations; therefore, the frontal area used in calculations were the maximum frontal area specified from the Shell Eco-Marathon guidelines. This will result in minor over compensation for various forces acting on the vehicle, but the motor horsepower calculated will be able to perform all functionality as specified.

Once all of the external forces have been accounted for, the moment required from the tire was calculated, so the motor torque was also calculated. Since the tire rpm is known, the motor rpm was also calculated. From these quantities, and necessary assumptions for the mechanical efficiency of the motor, the power required from the motor can was determined. The gear ratio must also be considered for these calculations. We are assuming a gear ratio of 5. Fortunately, the gear ratio chosen will not affect the amount of power that is required to propel the vehicle, but this will have an effect on the operating conditions of the motor. Since the urban competition is based on efficiency, the motor selection will affect the final decision on the overall gear ratio to better suit the operating conditions of the electric motor. After determining the power required for the application, the type of motor and the number of motors can were determined.

Utilization allowed for parametric analysis for each case. EES is particularly useful for parametric analysis when varying only one parameter. Code containing all constraints, assumptions, and equations can be produced to perform the calculations required for analysis. EES allows the user to produce parametric tables and plots of the desired parameters.

For various scenarios, the amount of force, torque, and speed can be calculated for the vehicle. For the sizing capability of the motor, a parametric analysis can be performed. The different cases that were considered were as follows:

- Case 1. Level ground with no acceleration (Fig. 15) (Steady State)
- Case 2. Level ground and acceleration of 2 mph/s
- Case 3. Incline of 5 degrees with no acceleration
- Case 4. Incline of 5 degrees with 2mph/s acceleration

From the analysis, motor sizing was determined based on the required functionality for the vehicle provided by the Shell Eco-marathon rules and track. The steady state for the application

can be considered as flat ground with no acceleration (Fig. 15). Plots for all other cases can be viewed in Appendix F.

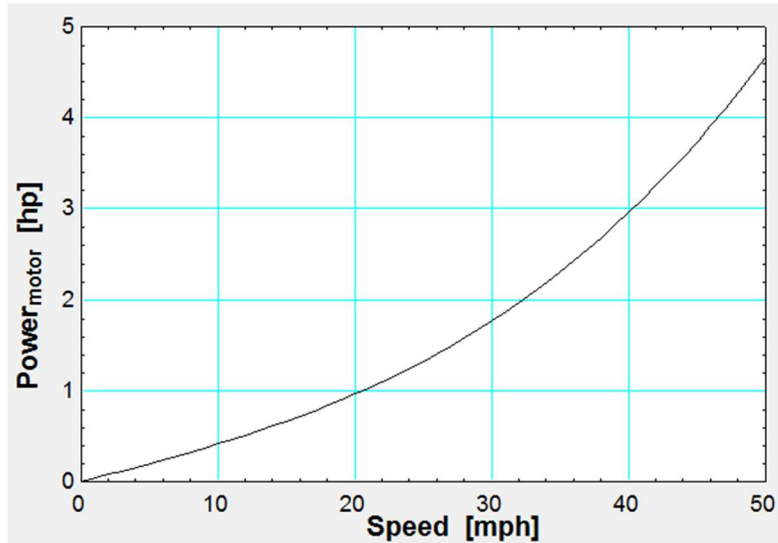


Figure 15. Power vs. Speed (Level Ground with no Acceleration).

Using this type of analysis, it was determined that a 2-horsepower motor would be optimal for the application. The vehicle will be able to meet the performance requirements of the Shell Eco-marathon. After determining the power required for the solar car, a decision on the type of motor had to be made.

Three options were considered for the motor(s) to be used on this vehicle. The choices were brushed direct current (DC), alternating current induction (AC), and brushless direct current (BLDC) motors. In addition to the type of motor, the decision to use one or two motors had to be made. To make this decision, the resulting effects on the drive train system had to also be considered. The use of one motor would increase the complexity of the drivetrain, decrease the vehicle's efficiency, and reduce the intricacy and cost of motor control. On the contrary, two motors would reduce the complexity of the drivetrain, increase the vehicle's efficiency, and increase the complexity and cost of motor control. Each option was evaluated with respect to these outcomes.

When considering brushed DC motors, permanent magnet DC (PMDC) motors were the focus. PMDC motors differ from other types of DC motors because of the permanent magnets in the field section instead of windings. A downside to this construction is that the field magnets can lose their magnetism over time resulting in lower torque production. Applications which require fast response time often use PMDC motors. This type of motor can deliver up to three hundred percent of its full load torque for short periods of time and is less expensive to operate than other DC motors due to the lack of field supply. In addition to delivering higher than rated torque, DC motors produce constant torque over a broad range of speeds [15]. Quick response time, high torque capability, and constant torque over a wide speed range fit the electric vehicle application, but there are several downsides to brushed DC motors. Reliability and maintenance are the two most critical issues with brushed DC motors in vehicle application. Specifically, the carbon brushes and commutator are uninsulated and susceptible to electric failure [15]. In this electric

vehicle application, carbon dust and moisture are the two biggest concerns. Both carbon dust and moisture provide conducting paths that can lead to shorting or grounding, resulting in low service life, maintenance costs, and reliability concerns.

As the name suggests, AC motors use alternating current. This alternating current causes the strength of the magnetic field to vary with the value of the current. The two main parts of an AC motor are the stator and the rotor. The stator is stationary and is made up of many electromagnets arranged to form a hollow cylinder. The rotor, therefore, is the rotating part of the motor and is mounted to the shaft. AC induction motors rely on magnetic induction to achieve rotation [16]. When current is applied to the stator, it causes a changing magnetic field which causes the rotor to rotate. Since rotation is caused by induction, the motor does not need a commutator or brushes, making it simple and durable. Therefore, AC motors are more cost effective in construction and ongoing maintenance. Additionally, AC motors for electric vehicle use often exceed DC motor performance [13]. Through eliminating the commutator and brushes, the AC induction motor is more efficient and reliable than a brushed DC motor, but for this application, converting AC current from a DC power supply and controlling the motor is much more complicated.

Brushless DC motors, like AC induction motors, are turned without the use of a commutator and brushes. However, they are powered with direct current controlled through a step controller rather than alternating current. BLDC motors closely resemble AC motors in construction, but retain many PMDC characteristics – high starting torque, linear speed/torque relationship – while offering higher efficiency without the brushes and commutator [13]. Again, the lack of carbon brushes and commutator grant a higher efficiency and great reliability with life expectancies of over 10,000 hours. Furthermore, they operate more quietly and with less electromagnetic interference than a conventional brushed motor. BLDC motors can be used in the same applications as brushed DC motors, but are often used for electric cars and model airplanes because of their high power to weight ratio [17]. BLDC motors meet nearly all of the demands of an electric vehicle.

Control Logic

From a macroscopic perspective, the control logic of any electric vehicle is essentially the same. There are several different types of motors and different ways to control them; the different components of an electric vehicle are integrated into a single system (Fig. 16).

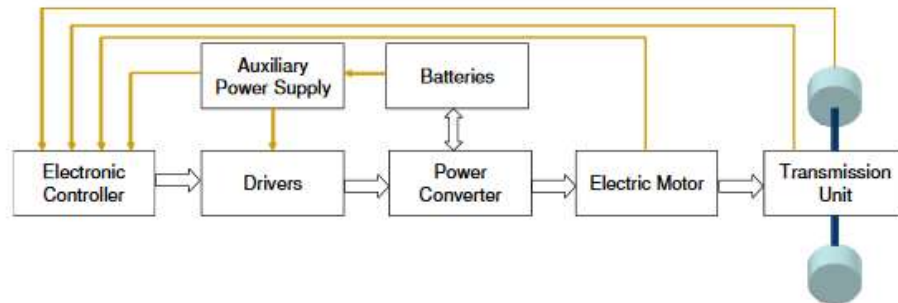


Figure 16. Major Components of an Electric Vehicle [18].

In the forward path (white arrows), the Electronic Controller provides information to the Drivers, which provides information to the Power Converter. The Power Converter provides information to both the battery and the Electric Motor, and finally, the Electric Motor provides information to the Transmission Unit, which turns the wheels.

In the reverse path (yellow lines), information passes from the Batteries to the Power Supply, which communicates to the Electronic Controller and the Driver. The Electric Motor, Transmission Unit, and wheels are all communicating information directly to the Electronic Controller. The wheels provide information back to the Electronic Controller via an instrument (usually a tachometer), so that the RPM's of the wheels can be adjusted according to the driver's desired output from information received via a user interface.

Given the wide variety of motors available on the market, the choice from a control standpoint was the motor type that was relatively simple, but that does not sacrifice too much efficiency—a DC motor. With a DC motor, the programming of the microcontroller will be simpler than with an AC induction motor. (Fig. 17) shows the complexity involved in controlling an AC induction motor.

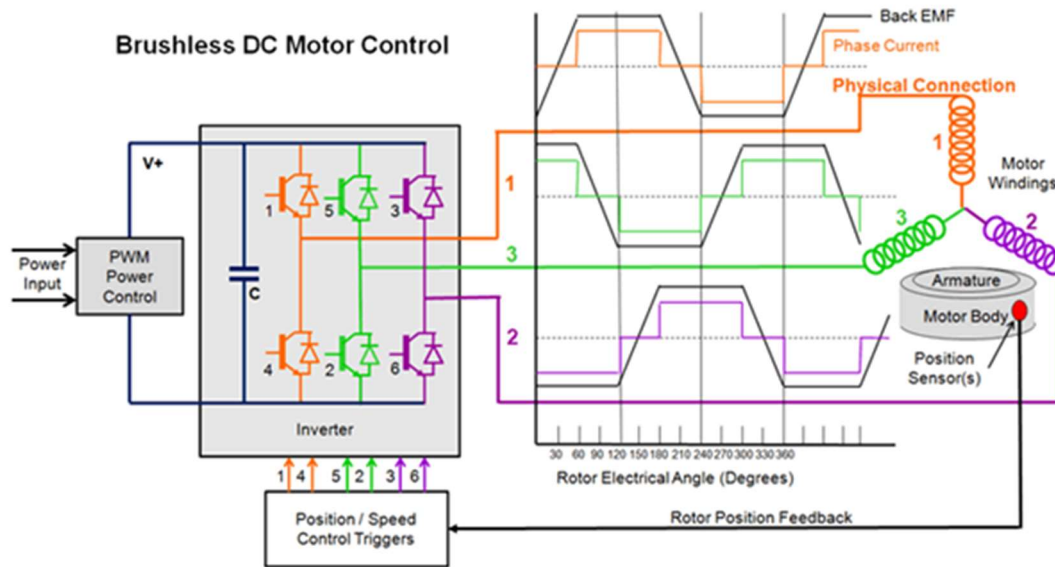


Figure 18. Controlling Voltage and Speed [19].

For programming of the varying current steps as a function of the rotor electrical angle, overlap of the phase current at varying angles must be timed accurately to obtain the desired back electro-magnetic force (EMF). Once a motor has been selected, this principle was researched in more detail, and implemented based on the specific characteristics of the motor.

For controlling the logic flow of the controller, the following diagram (Fig. 19) was useful as a foundation, but some steps can be omitted, depending on the requirements of the user.

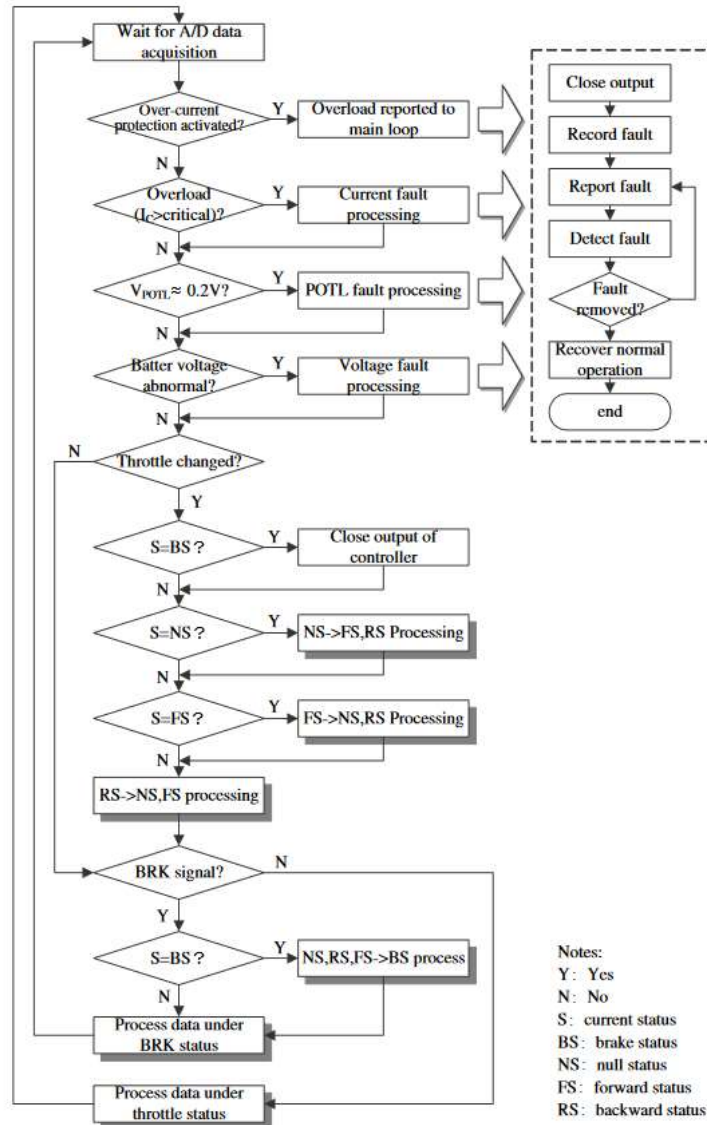


Figure 19. Operation of an EV Controller [18].

For the vehicle being designed, the faulting mechanisms feedback will be omitted initially to minimize complexity, but the principle will remain the same—if, for example, the overcurrent protection is activated, the program needs to end immediately.

Controlling two motors is not a linear progression, but the logic remains the same. Some components have to be added to the circuit to allow the motors to function in parallel. In order to have a two-independent rear wheel drive electric vehicle, the motors must be synchronized. Two of the same motors will still have some minimal inherent differences in peak torque and speed. To solve this problem, feedback from each motor would have to be interpreted by the vehicle's controller to synchronize the motors (Fig. 20).

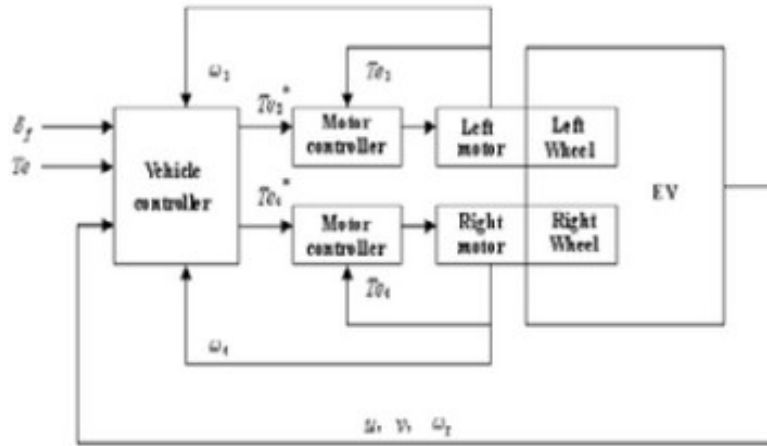


Figure 20. Independent Rear Wheel Drive Control.

Additionally, a vector control system would have to be implemented to achieve proper turning performance, stability, and driving wheel slip ratio [20].

Furthermore, a scaled motor controller prototype has been built to aid future teams in the task of building their own motor controller. Since the Shell Eco-marathon specifically says that teams must build their own motor controller, it was imperative that some work be done to set up future teams in this endeavor. However, this section of work proved to be extremely difficult for the mechanical engineering team members who worked on it, and it is recommended that the future work on the controller be completed by electrical engineering students. Nevertheless, a prototype of the controller was constructed using an Arduino Uno (Fig. 21) microcontroller. The board was hooked up to a breadboard (Fig. 22) that consisted of two push buttons that acted as circuit switches and a potentiometer that regulated speed of the small DC motor that was attached. One of the push buttons turned the motor on and off, the other push button changed the direction of spin for the motor's fan.



Figure 21. Arduino Microcontroller.

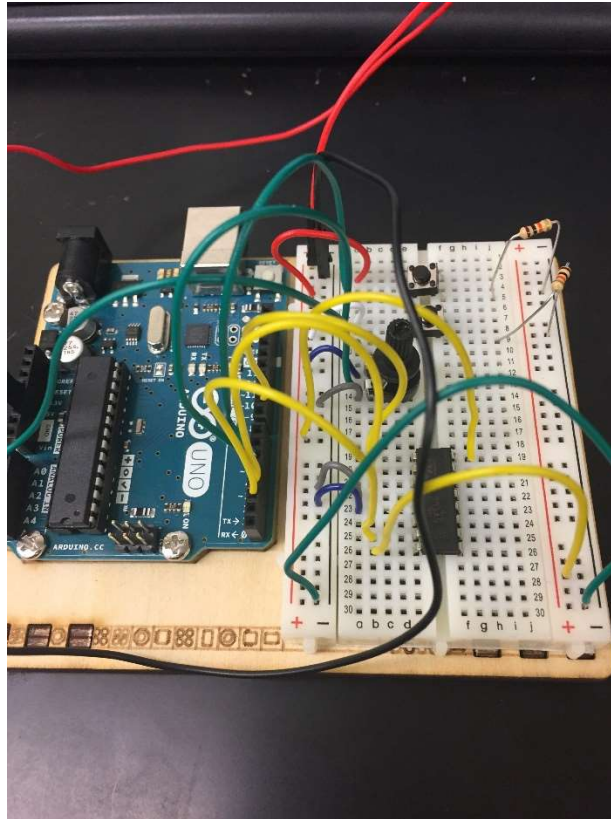


Figure 22. Arduino Breadboard with Potentiometer.

Steering and Suspension

The objective of this section of work is to design and implement a suspension system for the solar vehicle. This design must meet all Shell Eco-marathon urban concept and battery electric division specifications. Due to financial and time constraints, the suspension design must be simplistic in nature while offering maximum performance. This entails keeping the wheels in constant contact with the road at all times during cornering maneuvers while minimizing body roll. In doing so, friction between the tire and the road is maximized, ensuring maximum power transfer to the ground to propel the vehicle forward. Since the vehicle is to eventually be competed in the Shell Eco-marathon Urban Concept Battery Electric Division, passenger comfort is also an important design parameter.

The main function of a suspension system on any vehicle is to provide maximum friction between the tires and the ground. It also helps smooth out any imperfections on the road; therefore, limiting the impact's effects on the vehicle. This provides comfort to the driver and passengers while reducing forces exerted on the chassis. The suspension also provides stability while accelerating/decelerating and cornering.

The first step in designing the vehicle's suspension system is deciding which type of system to use. There are many types of suspension systems for different applications, each with their own advantages and disadvantages.

Once a system type was chosen, the suspension geometry was determined. This was accomplished with the help of a free online application called Vsusp. This program allows users to input geometric data and calculates several performance characteristics and results including swing arm length, camber gain, and roll center.

Using this geometry as a basis, components were modeled using SolidWorks. This program was also used for test fitting and analysis of components.

The double control arm system, specifically non-parallel unequal control arms, was chosen for the front-end suspension. This type of set up is used extensively in racing applications and high end performance vehicles. This is because the geometry of the double wishbone system allows for maximum tire-road contact during cornering or while traveling over road imperfections. It also allows for easy adjustments to various parameters including toe, camber, caster, and many others. If an error is made during the design of the suspension geometry, future design groups will be able to easily remedy it without totally redesigning the entire system. The double wishbone system contains more parts than other suspension types, making it more difficult to design and is generally more expensive to develop.

The first iteration of rear suspension design was modeled as a MacPherson strut type; this was later changed to the double wishbone system for various reasons. Since this vehicle's suspension geometry is unique, it became difficult to find a strut that was suitable. The upper mount for a typical MacPherson strut is fixed to the frame by several bolts. The mounting location on the frame is generally built into its design. Today's passenger vehicles use a unibody design which combines the chassis and main body into one structure. Our frame was developed before the suspension system; therefore, these mounting locations were not built into the frame. While it is possible to build attachment points onto the frame, they would likely become a critical failure point if poorly designed. The upper strut mount transfers most of the forces experienced by the suspension system to the frame. The MacPherson strut also uses a stabilizer bar between wheels of the same axle to reduce body roll. This component would also have to be custom made for this application. The geometry behind a stabilizer bar is surprisingly complex and would require many hours of research and design to develop.

The double wishbone design for the rear suspension solves all these issues. While suspension mounting locations will still have to be added to the frame, the forces transferred to the frame are distributed through several smaller mounts; allowing the use of smaller brackets. Shock length for rear suspension is within an inch of front suspension shock length, which allows us to use the same type of coil-over shock absorber. Double wishbone systems do not require a stabilizer bar as the MacPherson strut systems do, allowing the team to focus on other aspect of vehicle design and reducing overall cost.

The rear end contains the drivetrain components, therefore there were other considerations taken into account while designing the suspension system. In the front suspension, the shock absorber

mounts to the center of the lower control arm. The rear wheels, on the other hand, have a drive axle going through the upright knuckle. The drive axle lies on the same plane as the shock absorber so a different location was chosen. The rear shock absorbers will connect directly to the knuckles, slightly offset from the wheel centerline. This will create enough clearance for the drive axle without sacrificing performance.

In the designing this steering system there are two commonly used steering system to take into consideration, recirculating ball steering and rack and pinion steering system. The rack and pinion steering system are made up of a few components, the steering wheel, steering shaft, pinion, rack, tie rods, steering arm and steering knuckle (Fig. 23). This system is usually the most common given its simplicity in mechanism and why it was chosen for this project. A turn of the steering wheel causes the pinion gear to turn, moving the rack to the left or right depending on the direction of the wheel turn. But one must keep in mind that the wheel does not turn at the same degree as the steering wheel. The degree the wheel turns as a result of a given degrees turn of the steering wheel need to be considered [21].

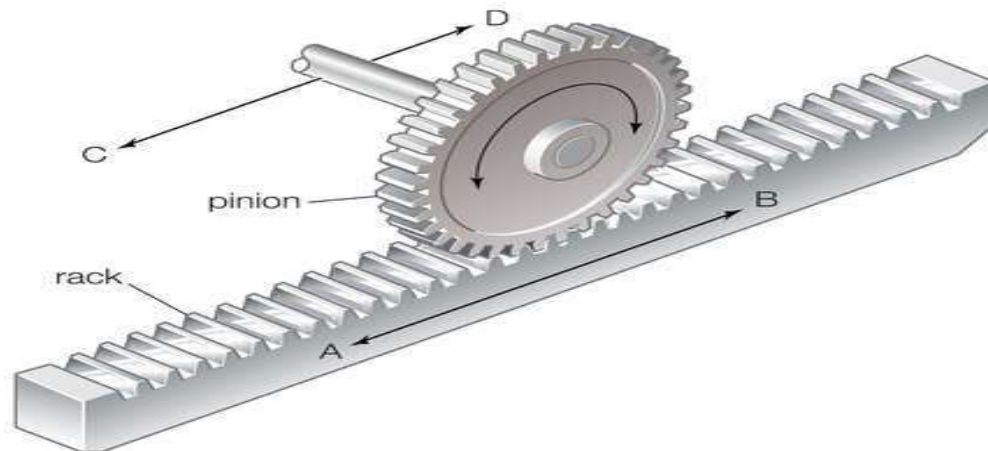


Figure 23. Rack and Pinion System.

Steering Ratio

A steering ratio is the numbers of degrees of turns of the steering wheel to the number of degrees of turn of the wheels as a result.

As an example, a motorcycle or a bicycle has a 1:1 steering ratio and this is because the steering wheel is fixed to the wheels. In general, a steering ratio of X: Y means that for every X turns (in degrees) of the steering wheel the wheel will turn Y turns (in degrees). So if one full turn of the steering wheel, 360 degrees, causes the wheel to turn 24 degrees, the ratio of turns is the $360:24 = 15:1$ [22].

High steering ratio means that it would take more turns to get the wheels turns but it makes for an easier turning. A low ratio means that the steering wheel is turned requires fewer revolutions

to get the wheel turning but requires more steering effort. Higher ratios are normally used for heavier cars while smaller cars not being so heavy does not require the higher mechanical advantage again of high steering ratio will normally use a low steering ratio. To get a sharper turn or more responsive turning it is best to use a low steering ratio. Race cars will typically have a very low steering ratio. This is because of the need for sharp cornering and quick turning response [22].

Variable steering ratio is another form of steering design that takes into account the advantages of both high and low steering ratios. In a variable steering ratio, the gear teeth on the rack and pinion is varied to achieve the required result. The rack teeth at the center are spaced very close and towards the ends the spacing are increased, so the control of the car will have a quicker response when the wheel is close to lock and less responsive when the steering wheel is close to the center position. This type of design is good for preventing oversteering while the vehicle is in high speed (Fig. 24) [22].

The steering ratio is also used in describing the ratio between the turning radius of an idle tire behavior and the actual turning radius of an actual tire behavior. A steering ratio value that is less than one indicates that the front wheel side slip is greater than the rear wheel which is the cause of under steering. Over steering is when the steering ratio is greater than one, an equal value such as the example of a motor cycle or a bicycle is considered a neutral steering. Counter steering, where the front wheel is turned to the opposite direction of the rear wheel is the result of a negative steering ratio.

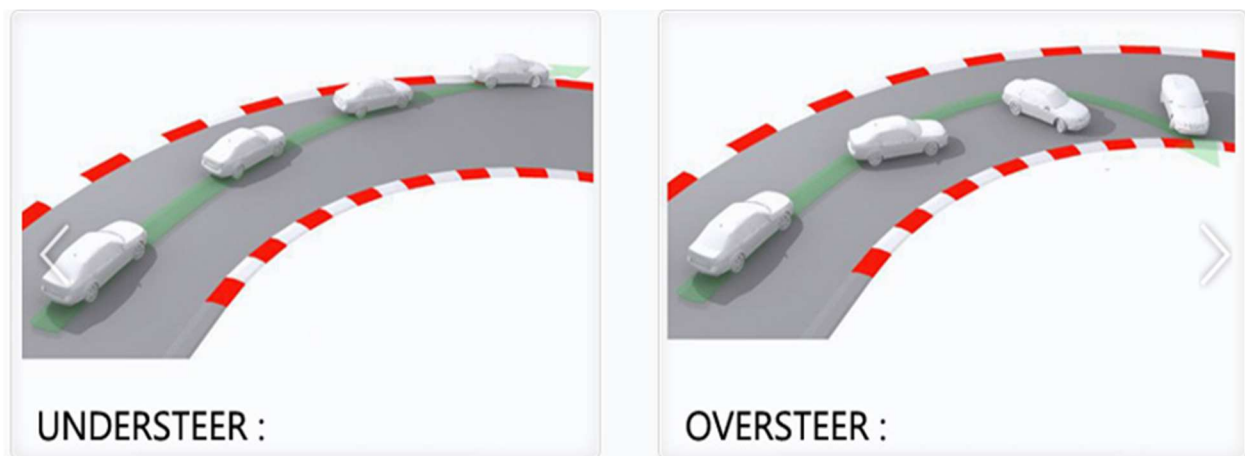


Figure 24. Understeering vs. Oversteering.

The Ackerman steering is based on the point of having a center point for which all your wheels will be turning on. This idea basically came of the need to correct tire slippage during cornering. This is what is the needed effect while a vehicle is cornering to prevent the vehicle from slipping while cornering. The inside wheel must trace a smaller radius than the outside wheel. If both wheel were to have the same degree of turn the inner wheel will not keep to the radius of the smaller circle. This would cause the inner wheel to scrub, slippage would occur. The radii of the inner and outer circle traced by the wheels during cornering are products of the car width and sharpness of the curve.

The geometry of Ackerman steering is defined by angling the steering arm such that a line drawn from both king pin through the steering arm will intercept at the center of the back axle. Below (Fig. 25) is a description of the Ackerman geometry, measured from the center of the tire to the angled steering arm. This steering system is best suited for the purpose of this design in that this design is for a small lightweight vehicle. This steering design will be composed of a rack and pinion system, inner and outer tie rods, steering arm, steering wheel and steering knuckle.

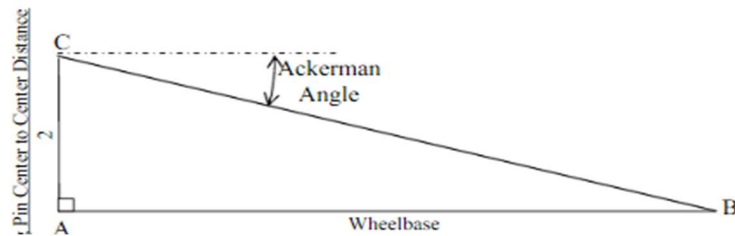


Figure 25. Ackerman Angle Depiction.

The image below is the basic configuration of the steering system that will be used in this design. The system at whole will include the suspension system of the car. Though not included (Fig. 26) in the illustration, it is also an important component to the handling and control of this design [21].

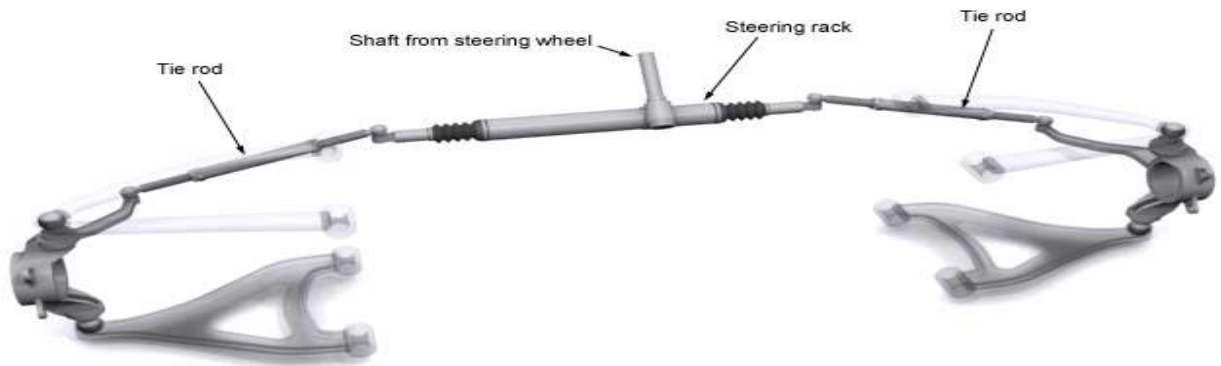


Figure 26. Assembled Steering System.

The suspension and steering systems directly affect the overall performance of the vehicle. Poor suspension design can result in excessive body roll, body squat/dive, bump steer, and other negative handling characteristics. The front-end suspension system will be a double-wishbone

system for its great handling characteristics. The rear suspension will be a McPherson strut. The design of this type of system is simpler than that of the double wishbone, however, the rear wheels are driven which introduces other design considerations and constraints. A rack and pinion system was chosen for the steering system due to its ease of design and adjustment. This type of steering is more efficient than the traditional mechanical linkages used in older vehicles. The increased efficiency and low target vehicle weight allow the driver to control steering without the assistance of power steering.

Results

Results were derived using a conservative manner. This section includes FEA, purchasing information, and parametric analysis.

Frame

As a starting point, it was important that the chassis had low center gravity and weight, fits general suspension system, and meets the competition requirements. Several designs of the frame were made, until a final design was selected (Fig. 27).

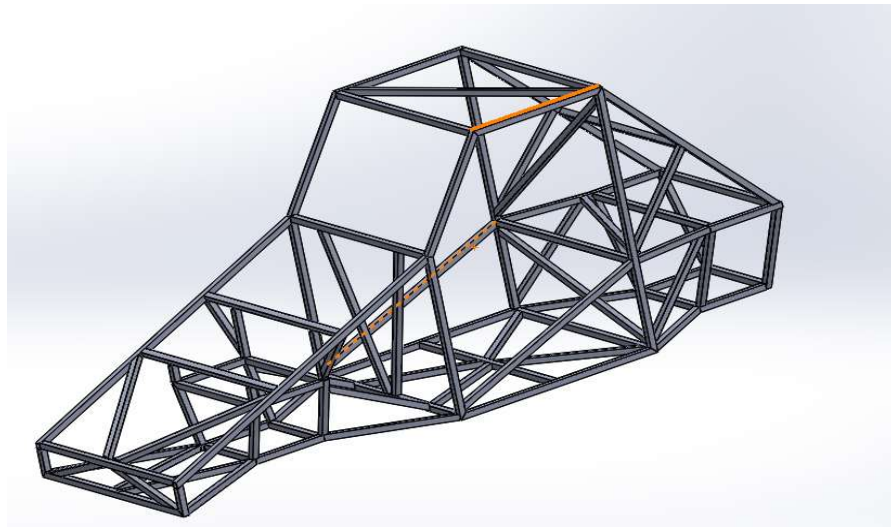


Figure 27. Final Chassis.

Analyzing the results for tension (Fig. 28, Fig. 29), the maximum stress can be determined. Tension of 5MPa obtained does not exceed the yield strength of 56MPa for Aluminum 6061. From that, it is concluded that the frame only suffers elastic deformation.

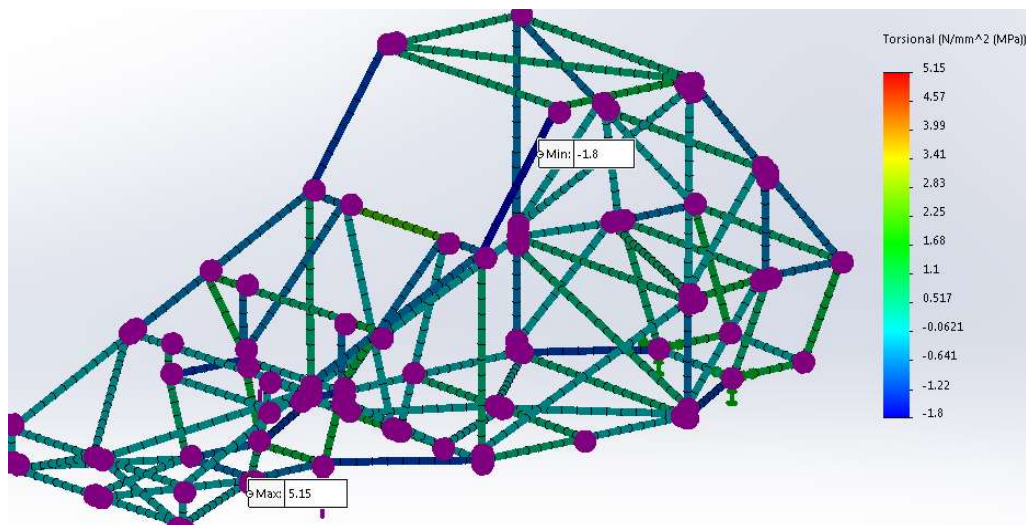


Figure 28. Results for Tension in MPa Unit.

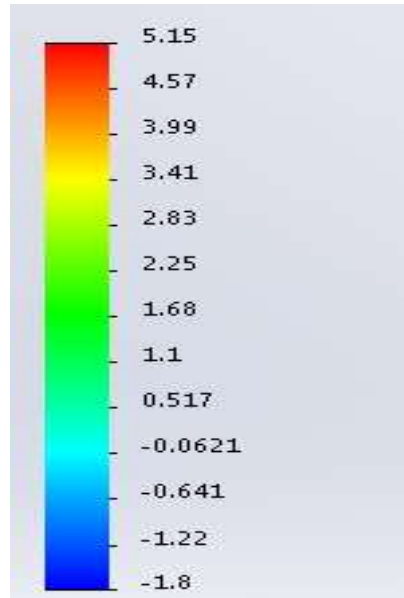


Figure 29. Results for Tension in MPa Unit.

For the torsional rigidity calculations, the values obtained (Fig. 30) are placed in the torsional rigidity equation presented before.

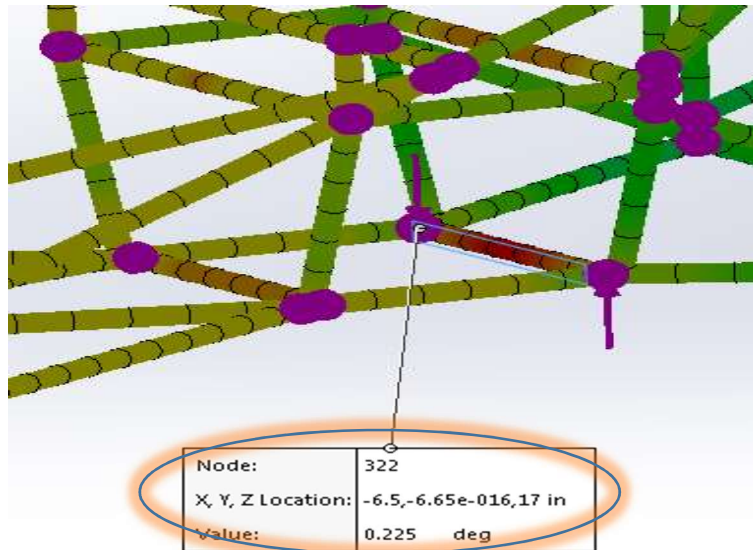


Figure 30. Results for Angular Deflection in Degrees.

Using the data retrieved, calculations were performed to determine the torsional rigidity as follows:

$$T = 2 * 1000 * \left(\frac{0.33}{2} \right) = 330Nm$$

$$\theta = 0.224 \text{ deg}$$

$$Kt = \frac{330}{0.224} = 1473 \text{ Nm/deg}$$

This shows that the solar car has a high torsional rigidity when compared with cars that are aimed to participate in a more intense competition. Typical values for torsional rigidity (Fig. 31) are shown below:

Vehicle	Chassis torsional stiffness
	[Nm/deg]
Formula SAE car	300 - 3000
Passenger car	5000 - 25000
Winston Cup racing car	15000 - 30000
Sports car	5000 - 50000
Formula One car	5000 - 10000

Figure 31. Typical values for Torsional Rigidity [23].

For roll bar analysis, the equivalent von Misses stress obtained in the x, y, and z direction is approximately 25MPa. This stress on the roll bar will not exceed the yield strength of 56MPa for Aluminum 6061. Based on this result, solar car's roll bar will not deform plastically when a 700N force is directly applied on it. Moreover, it has a factor of safety of 2.24. (Fig. 32, Fig. 33, Fig. 34)

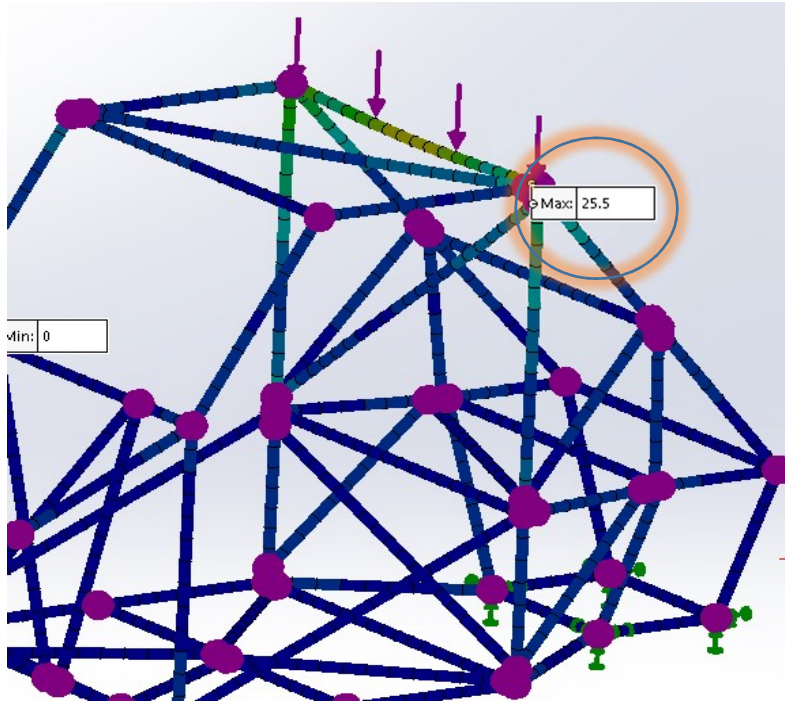


Figure 32. Max Result for Tension in Y Direction.

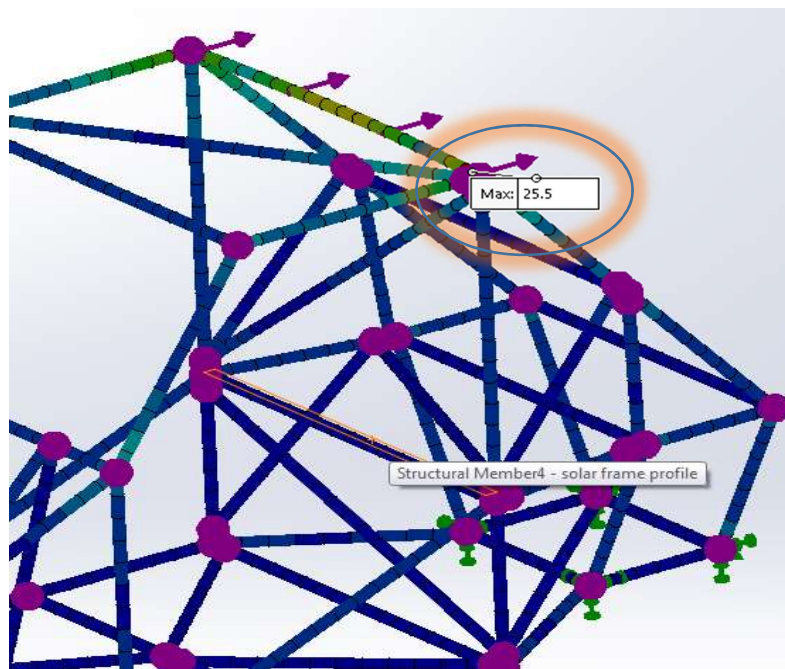


Figure 33. Max Result for Tension in X Direction.

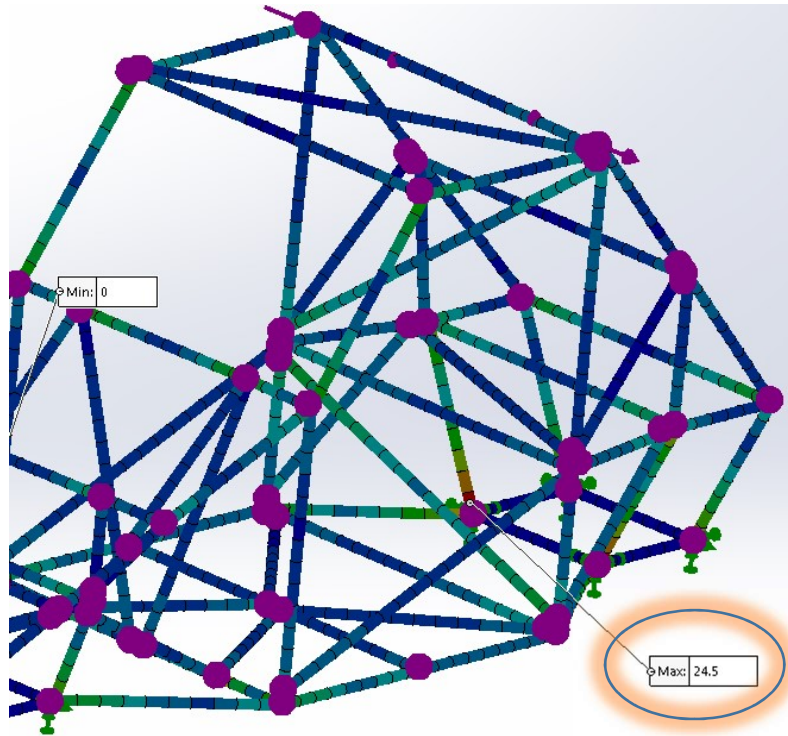


Figure 34. Max. Result for Tension in Z Direction.

Fabrication of Frame

From the generation of the BOM, it was determined that no additional raw material was needed. This was determined by summing the lengths of all the members and assuming that 20% of the material will be scrapped. Errors were expected due to student participation on the layout and preparation processes. Additionally, the welders are not cutting all material at once. Unfortunately, this will not result in the most efficient use of material, but due to spatial constraints on site, this is required process.

The team worked diligently with Arrow Pin & Product Inc. to produce the frame in a reasonable amount of time. Due to some miscommunication with the weld shop, frame welding was delayed dramatically. Since it was a volunteer job, it received the least amount of priority at the weld shop. If the weld shop got busy with work, the work on the frame was delayed further. The frame construction was concluded on April 24, 2017. Transportation was acquired to transport the frame back to the school. The component placements, such as motor and battery locations, were accelerated at this point in the project. It was clear what spatial constraints there are for specific components. This allowed the team to assure that a specific design will be suitable for the application. Working with the weld shop allowed the team members to obtain valuable experiential learning. Whether it was creating drafting materials (Appendix E) or providing manual labor (Fig. 8), the material learned will correlate over into real life application.

Powertrain

The process described in the Approach section was used to assess the feasibility of individual components. Calculations were performed to verify chosen components would not break under expected loading conditions.

General calculations determined that an optimum gear ratio of 2.6 would be suitable for the application; therefore, pulley diameters chosen were 3-3/4" and 9-1/4". The selected pulleys were designed for "V" belt drives.

A "V" belt was chosen based on the operating parameters. The design horsepower was determined given the operating horsepower and the service factor. The service factor corresponds to the application of the belt (Fig. 35). If the vehicle were to always run at top speed, an A size belt would be appropriate, but since the vehicle may be running slower, more torque will be present in the system; therefore, a B size belt was chosen. B size "V" belt parameters were then verified to allow for the pulley sizes previously stated.

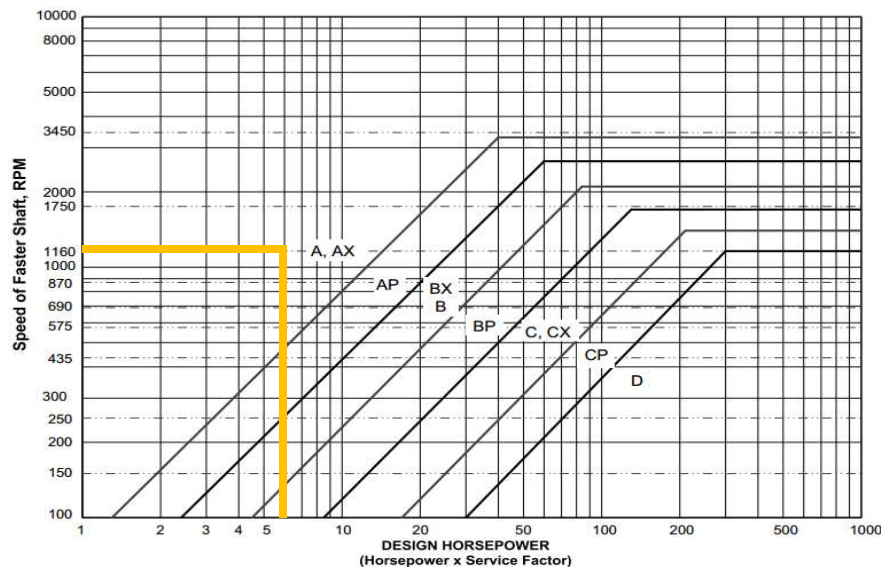


Figure 35. Belt Selection Chart.

Shaft size was determined based on the loading on the shaft. Dynamic loading due to the belt will result in higher forces than just static loading. Loading on the shaft is a function of belt speed, belt weight, driven pulley diameter, driver pulley diameter, design horsepower, and belt drive configuration. Once the dynamic loading on the shaft was determined, Modified Goodman Theory was applied to determine an appropriate diameter based on the material the shaft, the length of the shaft, and desired factor of safety. A shaft size of 1-1/2" was chosen with a corresponding 5.68 factor of safety. Reasons for such a high factor of safety include: unknown axial loading due to cornering force while turning, running key slot does not allow for adequate stress concentration calculations, and amount of vibrations on the shaft are unknown. The higher factor of safety will allow for the shaft to be safe even under some unknown working conditions.

Lastly, the bearings were selected. Working with the Formula SAE Team, SKF bearings were able to be retrieved at no cost. Bearing units were acquired for mounting purposes. Bearings were selected using the manufacturer's data. The worst case of loading was used to ensure that the bearings would be feasible for the application. These components were modeled using the SKF dimensions given in the catalogue.

All the component models were retrieved from McMaster-Carr or modeled. An assembly model was created to show how the components will be oriented (Fig. 36, Fig. 37).

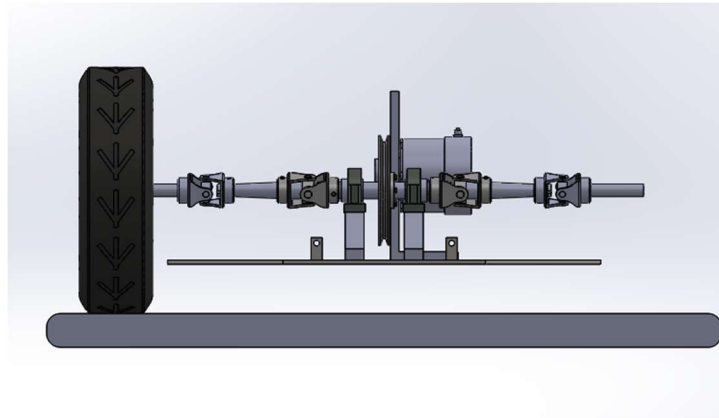


Figure 36. Powertrain 3D Model View #1.

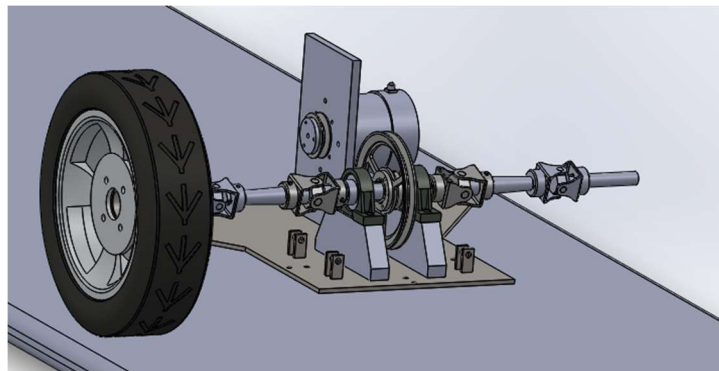


Figure 37. Powertrain 3D Model View #2

Solar Panel

Several solar panel experiments have been completed; the data can be taken from the software and input into MATLAB where the system estimation parameters can be determined. From these estimations, aesthetic graphs can be created that will easily show the extent of the capabilities of the solar panel. The graph below (Fig. 38) illustrates the current-voltage and current-power curves that were generated in Microsoft Excel using the data obtained from the solar analyzer scan when the panel was tested outside under direct sunlight. Important values (Table 1) that can be taken from this graph are illustrated below and were output directly from the solar analyzer. The panel was tested five times and the average values reflect these five tests (Appendix F).

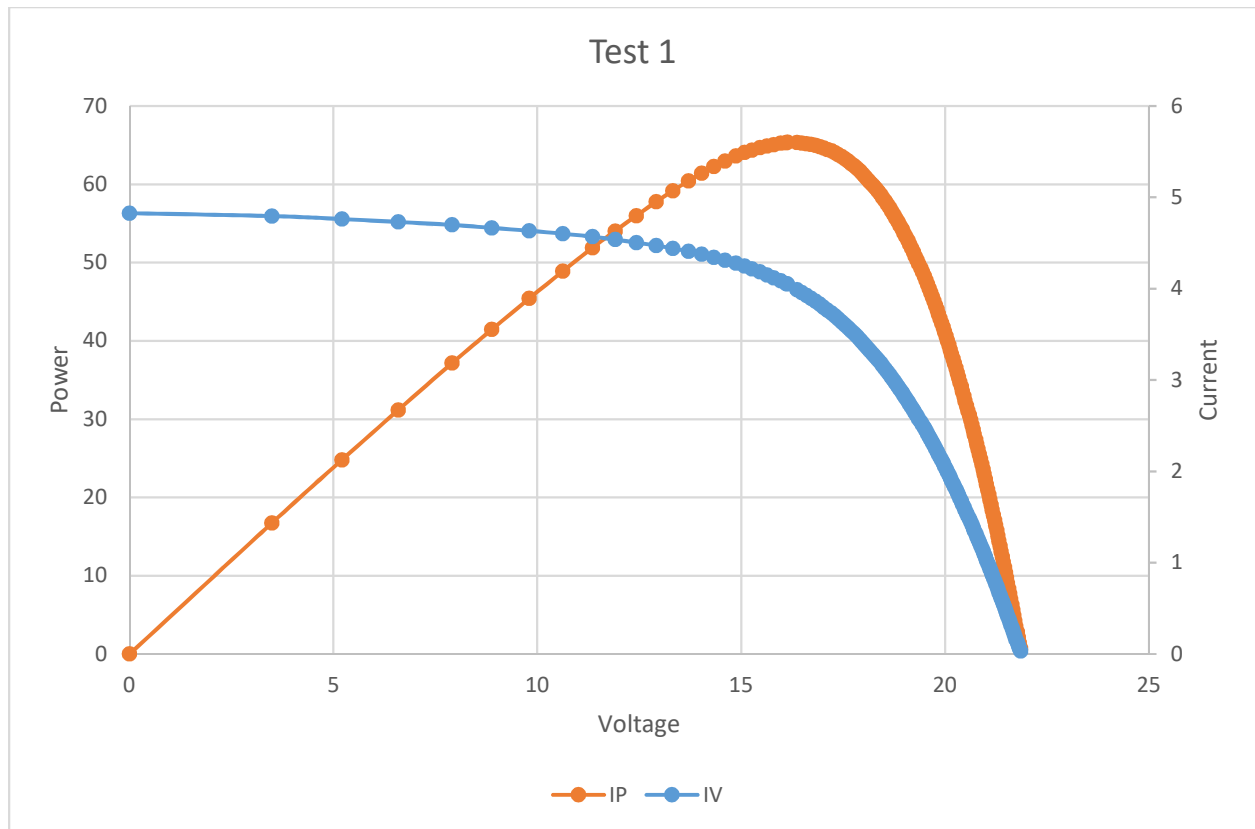


Figure 38. Solar Panel IV and IP Curves.

Table 1. Solar Panel Test Data.

	V _{open} (V)	I _{short} (A)	V _{maxp} (V)	I _{maxp} (A)	P _{max} (W)	Efficiency %
Test 1	21.86	4.827	4.052	16.13	65.39	26.56
Test 2	21.84	4.877	4.039	16.24	65.61	26.66
Test 3	21.78	4.781	3.92	16.23	63.65	25.87
Test 4	21.5	3.857	3.236	16.03	51.9	21.08
Test 5	21.58	4.33	3.577	16.16	57.81	23.46
Average	21.712	4.534	3.765	16.158	60.872	24.726

Battery

With the type of battery narrowed down to two types, deep cycle lead acid and LiFePO_4 , a comparison between the two can be made. As far as being charged by a solar panel, both of these batteries are perfectly capable. The first major difference between the batteries is the size and weight. The Lithium batteries are much smaller than lead acid, with Lithium on average having a volume that is approximately 80% smaller. For the size battery that is needed for this car, an average lead acid battery will be 50 pounds while an average Lithium battery will be approximately 20 pounds. The reduced weight and volume for the Lithium battery option offers a huge advantage. Making the vehicle lighter will make the efficiency and longevity increase. The rear of the vehicle is very small, so a smaller battery will be easier to place and mount. The most important comparison between the two batteries is safety. If a lead acid battery is over charged repeatedly over time Hydrogen gas can build up in the battery, and can explode if there is a short circuit within the battery. The chemistry of LiFePO_4 is inherently non-explosive, if a catastrophic failure occurs the battery will start on fire; it will burn hot, but will not explode. The BMS equipped with the battery would, in most cases, prevent this [27]. Lithium batteries offer roughly six times more cycles than lead acid. A typical lead acid battery can get 500 cycles, where a Lithium battery will give you approximately 3000 cycles. The number of cycles is dictated by the depth of discharge; the higher the percentage of discharge the less the batteries cycle life will be. The biggest strike against Lithium batteries is the cost. Lithium batteries are roughly three to four times more expensive than lead acid batteries. In the long run, the Lithium battery is a better value because they last six times longer. However, in the short term, the difference in price is a large obstacle. Taking into account all of these factors a final decision was made to go with LiFePO_4 despite the high cost. All of the advantages that come with the Lithium option far outweigh the large difference in price. Also, in the long run the decision will pay off when other groups are able to use it for years to come. It is also worth noting that this type of battery is required to compete in the Shell Eco-marathon, so this expense will not burden future groups.

A Lithium ion battery was determined to be the best option for this project. The first, and most important reason is safety. There are too many things that can go wrong with a lead acid battery. While the safety is reason enough, there are several other reasons as well. They are a fifth of the weight, easier to control, have a longer life span, are easier to charge, and are more efficient. The purchase of this battery will be an investment for future groups for years to come. With a final decision made on the type of battery that will be used, the actual battery itself can be now be evaluated. When deciding on a specific battery, the main factors used in the evaluation process were cost and power of the battery. The limit on the power of the battery, as per the rules of the Shell Eco-marathon competition, is one kilowatt hour. The motor that was picked was 48V, which makes the battery 48V as well. That would mean that any battery that is up to 20Ahr, but not much higher, would meet the requirement of the competition. Finding a LiFePO_4 battery that has one kilowatt hour of power, and is relatively cheap, is extremely difficult. The only way to get a battery customized to the parameters of the Shell Eco-marathon rule book and in our price range is to have it custom built. A custom 48 V, 20 Ah, battery was built and shipped to the school for \$820. This option is the best-case scenario because it comes with a personalized smart charger and BMS (Fig. 39, Fig. 40) that is built specifically for the battery.



Figure 39. Custom LiFePO₄ Battery with BMS.



Figure 40. Custom LiFePO₄ Battery Charger.

This will ensure a long battery life, and more importantly will make the battery safer because it can be guaranteed that the battery is being properly charged. The BMS will protect the battery from over charging, and will give early warning if anything is going wrong with the internal chemistry. A BMS is another requirement in order to participate in the Shell Eco-marathon competition, so purchasing this custom battery will ensure that the car can compete. A custom fit battery enclosure was also purchased (Fig. 41).



Figure 41. Custom Enclosure for Battery.

This will further increase the safety of the driver, not to mention protect the battery from the elements. All of this combined will lead to a long battery life that is safe for everyone involved.

In addition to the BMS, charger, enclosure, and characteristics of the battery, most importantly it can be charged by the solar panel. Research was completed to determine the appropriate method to charge the battery with the solar panel. With the help of the Morningstar TS-45 (Fig. 42) the battery can be efficiently and safely charged when the panel is in sunlight. This can be while the vehicle is operating or stationary. The charge controller can be programmed to use the same charging methods as the wall plug charger that is customized for the battery. Without the charge controller, the cells would be vulnerable to corruption due to improper charging techniques.



Figure 42. Morningstar TS-45 Charge Controller.

Motor and Control

Using an EES parametric analysis (Appendix G), it was determined that a 2.5 horsepower motor would provide sufficient power output to meet the demands of the competition. Given the complexity of the mathematics involved in the SVPWM of an AC induction motor, and the complexity this system would impose on the programming of the microcontroller, this type of motor was eliminated. A BLDC motor would be ideal for this type of application due to its high starting torque, constant torque over broad speed ranges, high power to weight ratio, and low maintenance. However, BLDC motors are significantly more expensive than brushed motors. Brushed PMDC motors offer the same benefits as BLDC motors, except they require more maintenance and are less efficient due to the presence of carbon brushes. Finally, given limited product availability and budgetary restrictions, a single 4 HP brushed PMDC motor kit was purchased along with a programmable controller. The decision to use one motor rather than two independently driven motors was made to reduce the costs and the control logic complexity at the expense of efficiency.

Powertrain Mounting

After selecting a motor and bearings, and receiving mechanical drawings, a powertrain mounting system was designed. Since the motor chosen was a C-face design – meaning the motor is mounted from the shaft side – and did not have feet, it could not be mounted to the bottom of the vehicle directly. Several iterations were made prior to selecting the final design for the motor mount. From the start, it was determined that wood would be used due ease of fabrication and modification, weight, and cost. The first iteration was large and had to be secured to the frame on two sides (Fig. 43). Additionally, there were concerns about rigidity while running the motor under load.

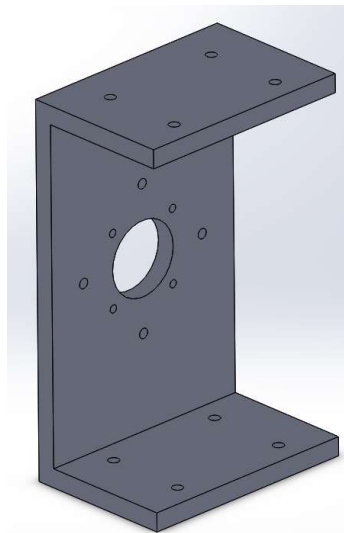


Figure 43. Motor Mount Design 1.

A second iteration was performed after the first (Figure 44). Slotted holes were added for alignment adjustments. The design was changed from a C shape to an L shape and angular supports were added for structural stability. The chosen motor was totally enclosed and not fan-cooled, so concerns about airflow and motor cooling arose with this design.

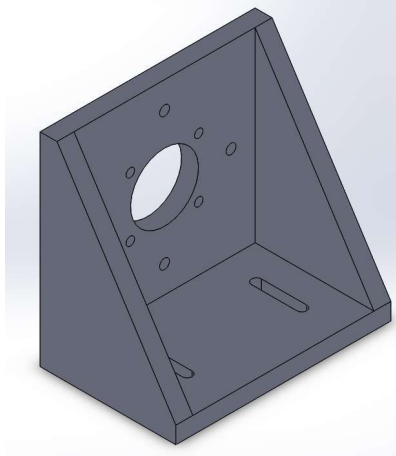


Figure 44. Motor Mount Design 2.

To remedy the issue of airflow around the motor, the plywood angular supports were replaced with steel corner braces to add structural rigidity, while opening space around the motor for cooling and retaining low weight. The final construction was completed with $\frac{3}{4}$ " Baltic Birch plywood (Fig. 45).



Figure 45. Motor Mount Final Design.

To raise the pillow-block bearings to the driven shaft height, a $1\frac{5}{8}$ " x $4\frac{1}{4}$ " x 7" Baltic Birch plywood riser was constructed (Fig. 46). Through-holes, $\frac{7}{16}$ " in diameter, were drilled $5\frac{1}{2}$ inches apart and symmetric about the centerline to fit the bearing holes. To secure the bearings and risers, a 6" x $\frac{3}{8}$ " bolt will be passed through the bearing, riser, and bottom plate of the vehicle and fastened with a nut on the underside of the car.

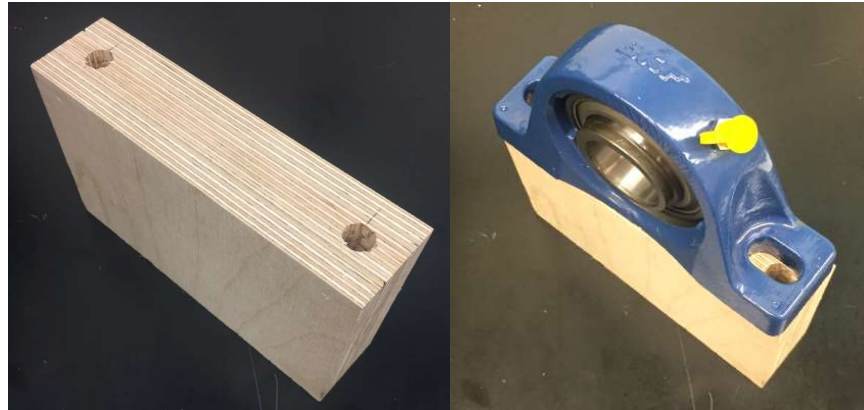


Figure 46. Bearing Risers.

Suspension and Steering

Decisions for this section were made considering finances, driver comfort, and adjustability. Handling was also a key factor in steering and suspension design.

Wheel Alignment Specifications

Design of the vehicle's suspension, steering, and frame began at the wheel. Wheel alignment was the first parameter considered in the systems' design. These parameters include toe, camber, and caster (Fig. 47) [25].

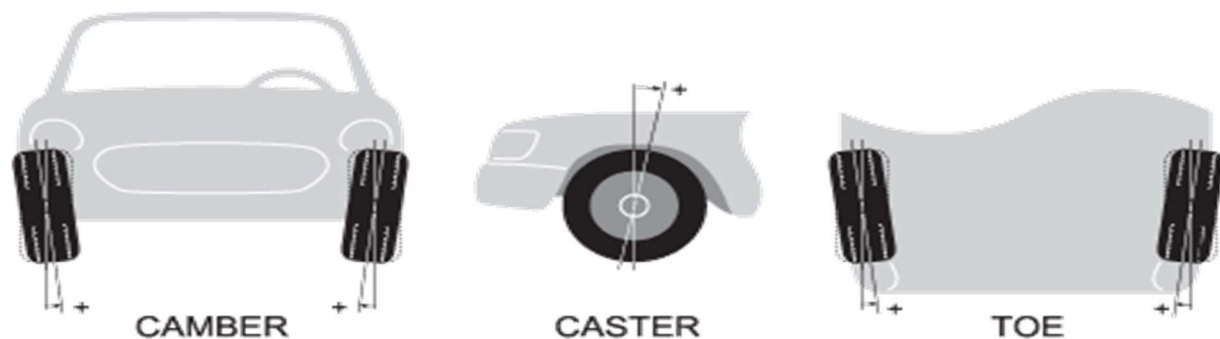


Figure 47. Wheel Alignment Parameters [25].

Most passenger vehicles today are designed with slightly positive toe (toe in), this is to compensate for the roads curvature, often referred to as “road crown”. The positive toe alignment helps keep the vehicle from drifting towards the road edge. However, the wheels are essentially fighting each other as the vehicle travels in a straight line. The solar vehicle will have a neutral toe angle to reduce friction losses at the wheel. The rack and pinion steering system chosen for the vehicle allows for easy toe alignment without purchasing or redesigning any components.

A neutral camber angle provides maximum contact between the tire and the road, so this situation is ideal. While toe angle is constant, the camber angle changes as the vehicle corners while the suspension articulates. During a turn, the outside wheels of the vehicle leans to the outside creating a positive camber angle, reducing road contact. The solar vehicle will have a slight negative camber as to counteract this effect. Camber angle also changes as a vehicle's

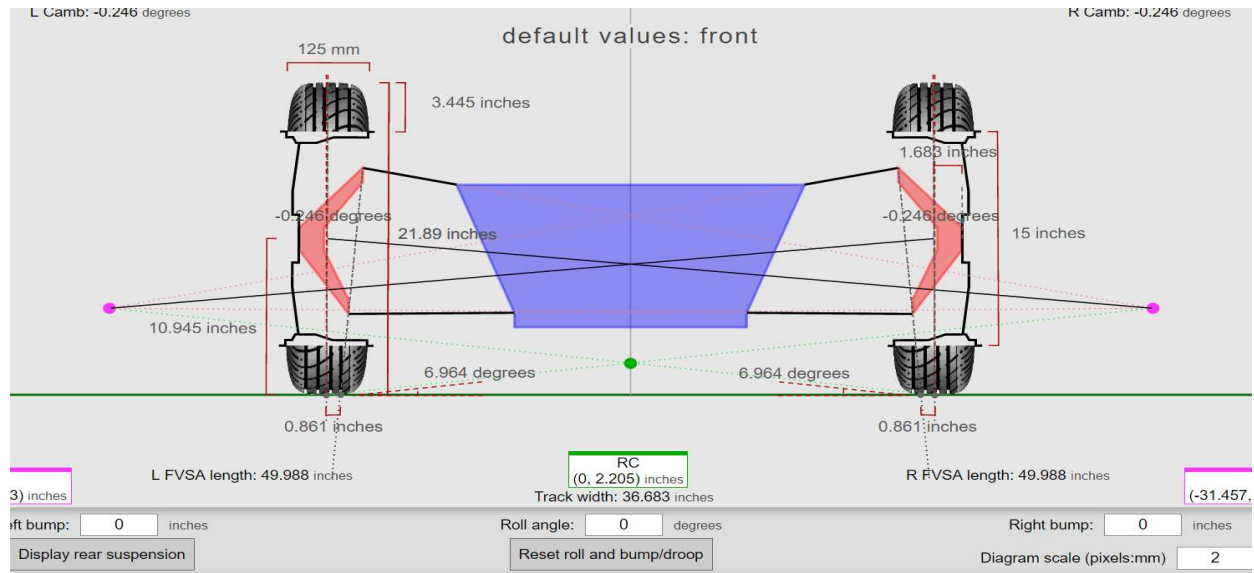
suspension articulates in response to road imperfections, accelerating/decelerating, and body roll. For this reason, the double wishbone system was chosen for the front-end suspension. The steering system is integrated into the front suspension; therefore, the suspension's performance greatly influences handling characteristics. Double wishbone set-ups allow the vehicle to maintain its camber angle as the wheel travels up and down. The rear suspension was chosen as the McPherson strut because of its ease of design and implementation. This system is less costly to develop than the double wishbone system yet still offers fully independent wheel travel. Caster is the measure of much the wheel tilts toward the front in relation to the suspension's center axis. Unlike toe and camber, desired caster is specific to a particular steering and suspension set up. Caster greatly affects steering effort and the stability of a vehicle while traveling in a straight line or cornering [25]. The solar vehicle will maintain a neutral caster angle to balance steering response and stability. Steering effort is not a concern since the vehicle will be lighter than 700 pounds and the large purchased steering wheel provides plenty of mechanical advantage.

Determining Optimal Geometry

Using the desired performance characteristics of the suspension and steering system, the overall geometry was determined using a web based application called Vsusp [26]. This program is a free suspension design tool which calculates parameters using static analysis. The simple interface allows the user to instantly see how the different components affect the overall behavior of the system. A program with dynamic simulation abilities would be ideal; however, this software is expensive and was not used due to financial constraints.

In addition to maintaining the desired wheel alignment listed above, there are several other parameters which greatly affect the handling characteristics of the solar vehicle including: scrub radius, steering angle inclination, change of roll center, and various others. These parameters must maintain acceptable values in response to wheel travel and body roll.

The picture below (Fig. 48) describes the input for wheel dimensions based on the physical measurements taken. Spare wheels for a commercial compact passenger are not ideal; they do offer plenty of negative offset (distance from the centerline of the wheel the mounting location of the hub) which allows for a greater range of freedom when designing components.



Every component influences the behavior of at least one other component, making the design process incredibly difficult without the use of parametric analysis. Instead a method of trial and error is used to determine frame dimensions, mounting locations of the frame, upper and lower control arm length, steering hub mounting locations, and ride height. In future work, parametric FEA analysis should be used to verify or correct the designs.

The performance characteristics were plotted against the roll angle of the body. Roll angle and wheel travel are used as the dependent variable in this analysis in order to compare the system behavior in response to driving conditions.

Spring Rate and Effective Wheel Radius

After the suspension and steering systems dimensions were designed, static analysis was performed on each wheel to determine the spring rate needed (Figure 49) as well as the effective wheel rate. Input parameters based on maximum vehicle weight and an overestimation of the unsprung weight is illustrated below (Table 2). Unsprung weight refers to the weight not supported by the suspension system including: wheel assembly, brake assembly, steering knuckle, and half the weight of the spring-damper assembly. Reducing unsprung weight greatly improves the handling characteristics of the vehicle.

Table 2. Spring Rate Input Parameters.

Estimated Total Vehicle Weight	700	lbs
Corner Weight (weight carried by each wheel)	175	lbs
Unsprung Weight (weight per corner not supported by suspension)	50	lbs

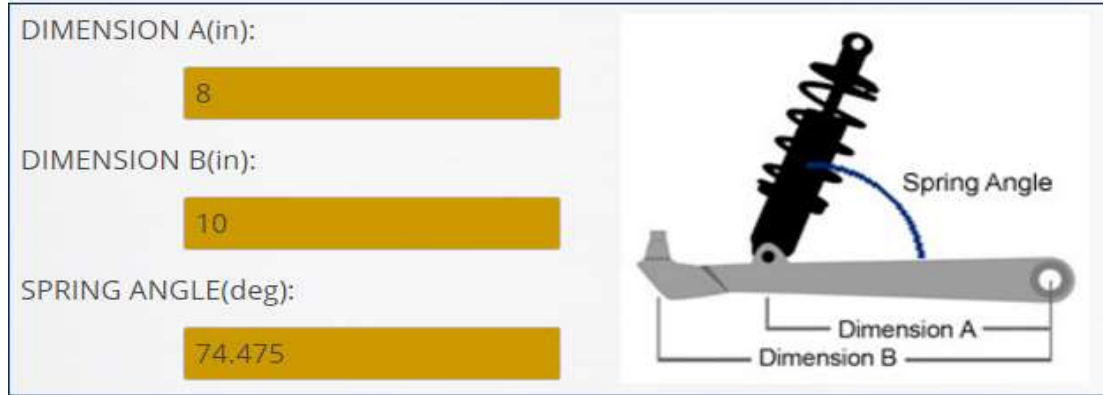


Figure 49. Input Parameters, Spring Rate [27].

The parameters were calculated (Table 3) using a spring rate calculator and verified with Microsoft Excel. Design considerations include: part clearance during articulation, resultant force applied to control arms and frame, and length of shock required [27].

Table 3. Spring Rate Results.

$\text{Sprung Weight} = \text{Corner Weight} - \text{Unsprung Weight}$	125	lbs
$\text{Motion Ratio} = \left(\frac{\text{Dimension A}}{\text{Dimension B}} \right) * \sin(\text{Spring Angle})$	0.771	
$\text{Static Load} = \frac{\text{Sprung Weight}}{\text{Motion Ratio}}$	162.17	lbs
$\text{Spring Rate} = \frac{\text{Static Load}}{\text{Shock Ride Height}}$	51.32	lbs/in
$\text{Effective Wheel Rate} = \text{Spring Rate} * \text{Motion Ratio}^2$	30.49	lbs/in

Changing the mounting location of the shock in relation to the frame offers a single solution to these considerations. By creating an offset of 2 inches to the outside of the frames side allows the shock to retain its vertical position while also decreasing the total length of the shock. This offset also allows space for the bracket required to attach the steel suspension components to the aluminum frame.

The overall design process for the steering and steering systems is nearly complete. All of the important dimensions and performance parameters have been determined; from the selection of system to be used, to the specific offset for frame mounting. The next step is to complete the modelling of the individual components in CAD. With the components modeled, an assembly model gave detailed information on how the components will physically fit together. Prototypes of each component will be 3-D printed to verify these findings. Fasteners and joints can be purchased based on the dimension of these final prototypes. Once all clearance issues have been addressed, fabrication of the custom parts can be arranged (control arms, steering knuckle).

Assembly of the suspension and steering assembly can begin as soon as all parts have been fabricated and purchased.

Fabrication of Steering Components

Most of the components for the steering system were already purchased by the previous team. However, it is necessary to adjust some of those components to fit the solar vehicle's conceptual design. For example, the steering column is one of the components that needed to be adjusted to fit the new frame design to allow room for the driver. Since the steering knuckle and steering mounts were not purchased, and have a customized design, it is necessary to fabricate them.

In order to avoid waste of resources and to better visualize the steering knuckle, a 3D printing replica of it was made. For this task, the MakerBot Replicator (Fig. 50) and its software were utilized, which converts the SolidWorks file of the steering knuckle to a file that can be read by the 3D printer.



Figure 50. MakerBot Replicator.

Since the steering knuckle dimensions were not ideal for this specific 3D printer, it was divided into 3 parts and printed separately. After having the 3 parts printed, they were glued together to form the actual part (Fig. 51).

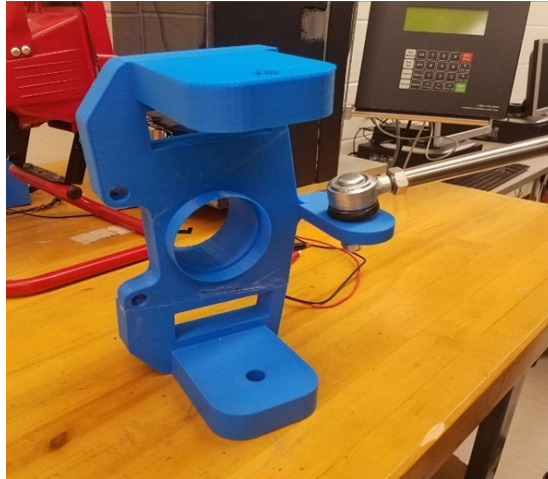


Figure 51. 3D Printed Steering Knuckle.

The next step for future teams is to actually manufacture the steering knuckle. This can be done either using a CNC machine or using different manufacturing machines, such as a lathe and mill.

As mentioned before, it is necessary to modify the steering column to fit the newly designed steering system. Since this part is longer than what is needed, a simple cut will suffice (Fig. 52).



Figure 52. Cut Location of Steering Column.

To mount the steering column to the frame, a plate (Fig. 53) will be bolted to the front of the frame using a U-bolt.

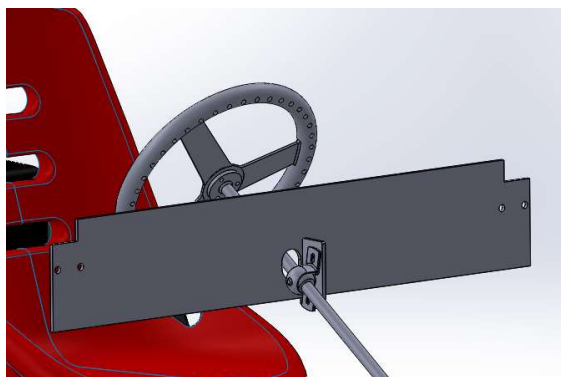


Figure 53. Plating for Steering Column Mounting.

The choice of using a U-bolt is to avoid weakening the frame by drilling into it. The plate will have a hole where the column will be fitted using a bushing (Fig. 54). The rack and pinion will be mounted to the suspension plate using a standard bolt.



Figure 54. Steering Column Bushing.

An important aspect of these mechanical designs is the choice of fastener for each joint. 304 stainless steel was chosen as the bolt material for various reasons. 304 stainless steel is the most common stainless alloy; it has acceptable mechanical properties (tensile strength, ductility), is resistant to oxidation, and is reasonably priced. Resistance to oxidation was a major consideration for the material of the shoulder bolts which connect the control arms and shock absorbers to the frame brackets. In this application, the bolts are fixed while the suspension components rotate around the unthreaded shoulder of the bolt. The chemical composition of stainless steel prevents it from scaling as quickly as other alloys, this also prevents the eyelets/rod ends from seizing and breaking.

The control arms are to have $\frac{1}{2}$ " standard coarse thread (UNC) cut externally to fit the female shank rod end. The rod end has a Nylon insert that reduces need for lubrication and acts to dampen vibrations from the suspension to the frame. The other end of the control arms that connect to the steering knuckles use a sealed, greased ball joint which are commonly used in production vehicles. This is a tried-and-true design that allows for suspension and steering system articulation. The following picture depicts the front suspension and steering assembly and includes all major components of each respective system (Fig. 55).

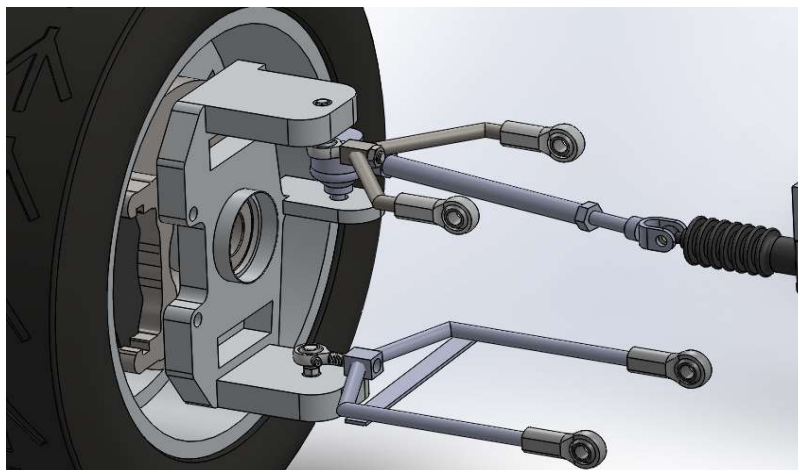


Figure 55. Front Suspension and Steering Subassembly.

Securing the suspension components to the frame requires adding brackets since there are no mounting locations in the original design. The frame is 6061 Aluminum while the mounting brackets were chosen as 1018 carbon steel. Welding dissimilar metals is not ideal and may lead to failure at the joint, therefore, a plate is fastened to bottom and top suspension sections (front and rear) of the frame using U-bolts. This allows the brackets to be welded to the plate rather than the frame itself. The plates also become a mounting location for other vehicle components. The downside to the plate concept is weight. The current design is as simplistic as possible to reduce fabrication costs. Once all the vehicles components have been located within the chassis, future design teams will be able to machine away excess material. Pictured below is an example of one such plate (Fig. 56).

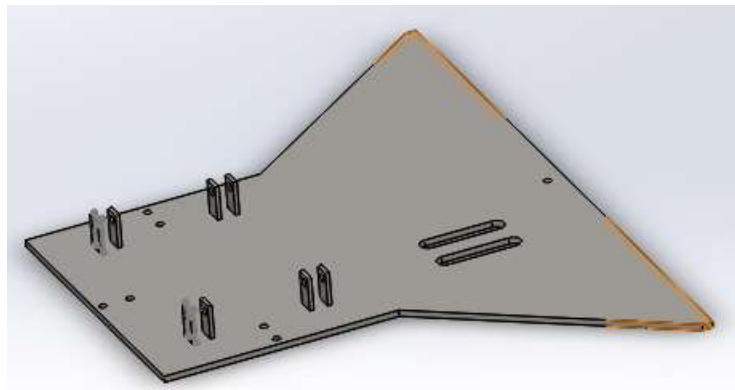


Figure 56. Rear Lower Suspension Plate.

Conclusions

The solar vehicle 1st iteration design is completed. This was accomplished by designing all of the subsystems individually and integrating them into a final design. These subsystems consist of the following:

- Frame – Design and Fabrication of the vehicle frame.
- Steering – Design and 3D Printing of Steering Knuckles & Modeling of Acquired Components.
- Suspension – Design of Control Arms Mounting Locations.
- Drivetrain – Motor Controller Programming, Design of Drivetrain, and Fabrication of Test Stand.
- Power – Solar Efficiency Test & Purchasing Charge Storage Devices

Components that were needed to meet objectives were purchased and prioritized. The primary components acquired were as follows with their respective features:

- Frame – Fabrication was completed and transported to campus.
 - Used in conjunction with plating scheme to mount components.
- Battery – Purchased and Received with charger and enclosure.
 - Used for energy storage from Solar or direct electricity input.
- Motor/Motor Controller – Purchased and Received with accessories.
 - Used for vehicle propulsion and limit the speed output of the motor.
- Charge Controller – Purchased and Received.
 - Used to convert DC to AC voltage and prevent harmful charging phenomena to the battery.

Supplemental materials were purchased to accommodate the project and its future endeavors. A full inventory was produced by creating interactive Microsoft Excel worksheets. Inventory may be sorted in many different combinations. In addition to components that were already acquired, components that were used for design, but were not purchased, were included in the list as well. This list has been labeled “Master Component List.” Screenshots from the Master Component List may be seen in Appendix B.

In the future years, emphasis should be on the optimization and fabrication of the entire vehicle. The current model (Fig. 57, Fig. 58) should be used as a starting point. The first iteration design was meant to be flexible to allow variations in design and component configurations. Before beginning any new designs, research to ensure that designs will accommodate the rules of the Shell Eco-marathon. New component configurations should be explored and evaluated. If current design configurations are used, efforts should be focused on FEA analysis to verify the safety and validity of the design. Upon completion of FEA, fabrication processes should be considered and progressed. Also, new components such as seat belts, headlights, foot pedal, wind shield, wind shield wipers, reverse break lights, and doors. Project objectives were accomplished with considerations with next year’s team ease to pick up progress.

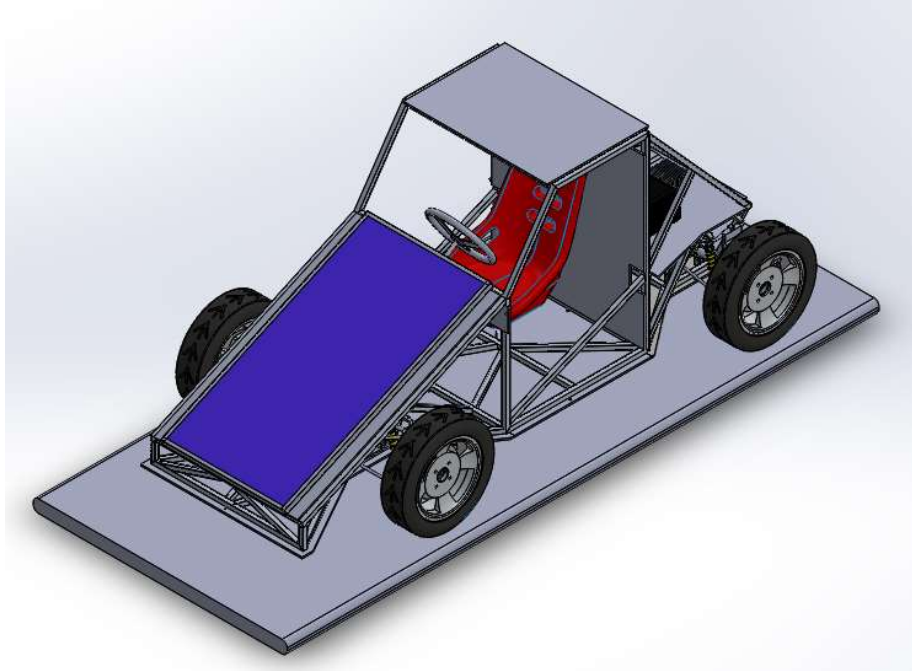


Figure 57. Orthogonal Assembly View 1.

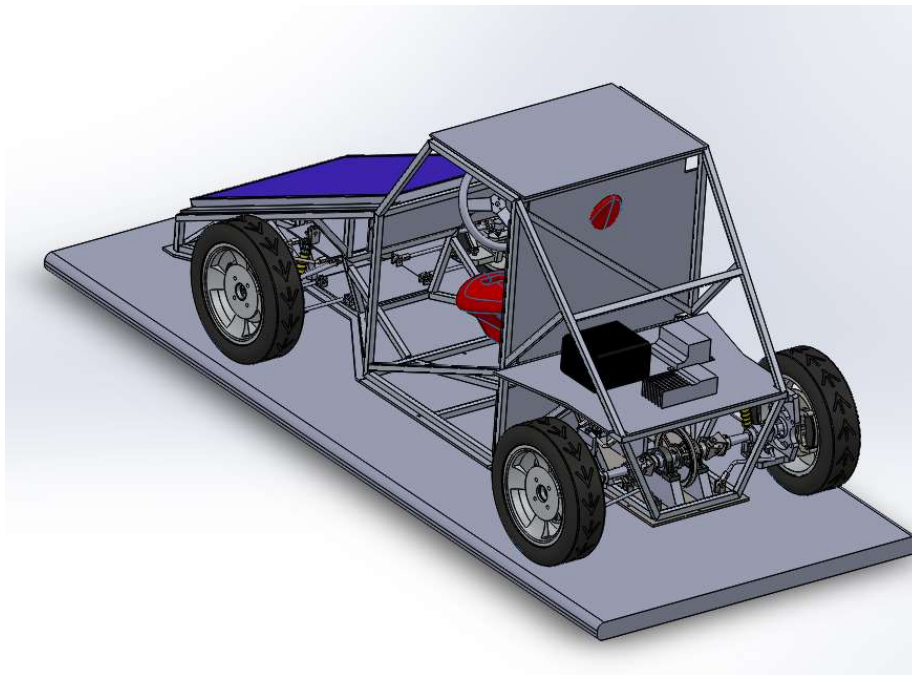


Figure 58. Orthogonal Assembly View 2.

References

- [1] "Greenhouse Gas Admissions," EPA, 06 10 2016. [Online]. Available: <https://www.epa.gov/ghgemissions/sources-greenhouse-gas-emissions>. [Accessed 22 11 2016].
- [2] Shell Global, "Official Rules Chapter," 2016. [Online]. Available: <http://www.shell.com/energy-and-innovation/shell-ecomarathon/for-participants/rules-and-competition-overview.html>. [Accessed 1 September 2016].
- [3] F. Beer, E. D. Johnston and D. Mazurek, *Mechanics of Materials*, New York: McGraw-Hill Education, 2015.
- [4] G. Weiss, "Analise Computacional e Experimental de Rigidez a Torcao de um Chassi de Formula SAE," Rio de Janeiro, 2010.
- [5] W. Milliken and D. Milliken, *Race Car Vehicle Dynamics*, Warrendale: Society of Automotive Engineers, 1995.
- [6] W. Riley and A. George, "Design, Analysis and Testin of Formula SAE Car Chassis," in *Motorsports Engineering Conference and Exhibition*, Indianapolis , 2002.
- [7] G. Knier, "Science Beta," 06 August 2008. [Online]. Available: <https://science.nasa.gov/science-news/science-at-nasa/2002/solarcells>. [Accessed 22 November 2016].
- [8] B. Darden, "Battery Basics," 22 January 2012. [Online]. Available: <https://www.batterystuff.com/kb/articles/battery-articles/battery-basics.html>. [Accessed 27 October 2016].
- [9] Cadex, "Understanding Lithium Ion," 3 May 2016. [Online]. Available: http://batteryuniversity.com/learn/article/lithium_based_batteries. [Accessed 6 Novemver 2016].
- [10] Cadex, "Types of Lithium-ion," 7 October 2016. [Online]. Available: http://batteryuniversity.com/learn/article/types_of_lithium_ion. [Accessed 1 November 2016].
- [11] Motor Challenge a Program of the U.S. Department of Energy, "Fact Sheet: Determining Electric Motor Load and Efficiency," U.S. Department of Energy.
- [12] National Instruments, "Vehicle Performance Analysis," 22 December 2015. [Online]. Available: <http://www.ni.com/white-paper/13014/en/>. [Accessed September 2016].
- [13] S. Leitman and B. Brant, *Build Your Own Electric Vehicle*, Third ed., New York, New York: McGraw-Hill Education, 2013.
- [14] J. Wong, *Theory of Ground Vehicles*, 4th ed., Honoken,, New Jersey: Wiley & Sons, 2008, pp. 221-226.
- [15] Galco Industrial Electronics, "DC Motors - Advnatages and Hazards of Running DC Motors," [Online]. Available: <https://www.galco.com/comp/prod/moto-dc.htm>. [Accessed 12 October 2016].
- [16] Galco Industrial Electronics, "AC Motor Diagrams - Basic Stator and Rotor Operation," [Online]. Available: <https://www.galco.com/comp/prod/moto-ac.htm>. [Accessed 12 October 2016].
- [17] NMB Technologies Corporation | A Minebea Group Company, "Brushless DC Motors," Minebea Co., LTD, [Online]. Available: <http://www.nmbtc.com/brushless-dc-motors/why-brushless-motors/>. [Accessed 12 October 2016].
- [18] J. L. a. Y. C. Qi Huang, "Control of Electric Vehicle," in *Urban Transport and Hybrid Vehicles*, Chengdu, Sichuan, Sciyo, 2010, pp. 163-190.
- [19] "Battery and Energy Technologies," [Online]. Available: <http://www.mpoweruk.com/motorsbrushless.htm>. [Accessed November 2016].
- [20] G. Li, W. Hong, D. Zhang and C. Zong, "Research on Control Strategy of Two Independent Rear Wheels Drive Electric Vehicle," *Physics Procedia*, vol. 24, pp. 87-93, 2012.
- [21] C. J. Longhurst, " Christopher J Longhurst," [Online]. Available: http://www.carbibles.com/steering_bible.html. [Accessed 20 november 2016].
- [22] H. B. Pacejka, in *Tyre and vehicle dynamics*, Butterworth-Heinemann, 2006.
- [23] G. Weiss, "Analise Computacional e Experimental de Rigidez a Torcao de um Chassi de Formula SAE," Rio de Janeiro, 2010.
- [24] PowerTech Systems, "Lithium Iron Phosphate (LiFePO4)," PowerTech Systems, 2016. [Online]. Available: <http://www.powertechsystems.eu/home/tech-corner/lithium-iron-phosphate-lifepo4/>. [Accessed 20 November 2016].
- [25] "Wheel Alignment Guide," Ford Motor Company, [Online]. Available: <http://www.fivestarfordga.com/blogs/1371/warner-robins-ford-service/ford-wheel-alignment-guide/>. [Accessed 2 December 2016].
- [26] "Vsusp," [Online]. Available: <http://www.vsusp.com>. [Accessed November 2016].

- [27] "Spring Rate Calculator," MW Industries, [Online]. Available: <http://www.hypercoils.com/spring-calculator>. [Accessed 20 11 2016].
- [28] R. Singh, "Structural Performance Analysis of a Formula SAE Car," *Jurnal Mekanikal*, no. 31, pp. 46-61, 2010.
- [29] K. Nice, ""How Car Steering Works"," 31 May 2001. [Online]. Available: <<http://auto.howstuffworks.com/steering.htm>>. [Accessed 5 december 2016].
- [30] "www.motor.org.uk," September 2009. [Online]. Available: https://web.archive.org/web/20130518220840/http://www.motor.org.uk/documentlibrary/Sep%2009/TT%20_%20Sept%2009.pdf. [Accessed 5 December 2016].
- [31] "www.quora.com," [Online]. Available: <https://www.quora.com/Which-kind-of-steering-system-should-be-used-in-go-kart>. [Accessed 05 December 2016].

Appendix A: Previously Retrieved Components

These were materials acquired from previous groups.



Driver Seat



Steering Components



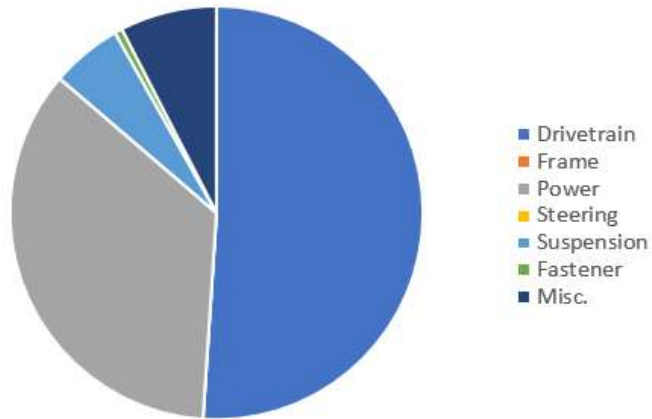
4 Wheels



Solar Panel

Appendix B: Solar Vehicle Stock Information

Cost Breakdown of Acquired Materials



Acquisition Status

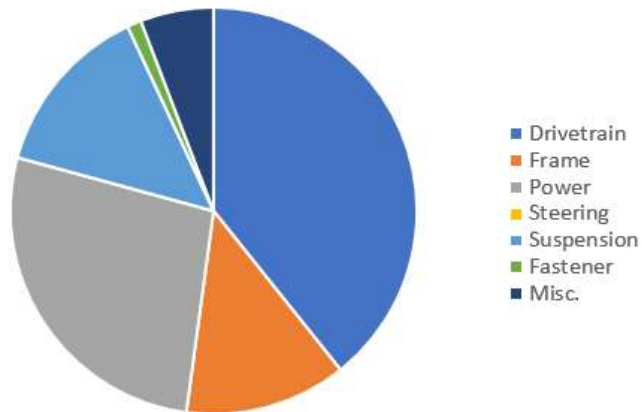
In Stock

In Transit

To Be Purchased

Drivetrain	51.04%
Frame	0.00%
Power	35.22%
Steering	0.00%
Suspension	5.56%
Fastener	0.61%
Misc.	7.57%

Cost Breakdown of All Materials



Acquisition Status

In Stock

In Transit

To Be Purchased

Drivetrain	39.26%
Frame	12.89%
Power	27.09%
Steering	0.00%
Suspension	13.81%
Fastener	1.13%
Misc.	5.82%

Drivetrain	Sum of Quantity
Arduino Uno	1
Zip Ties	10
MotoEnergy ME0909 Drive Kit (Motor Kit)	1
Foot Pedal	1
Alltarx SR4830 Controller	1
GigaVac GX14 Contactor	1
6AWG Wire Kit	1
Fuse & Holder	1
CycleAnalyst Display w/ 300A Shunt	1
SH Bushing-Bore Pulley, 3.75" OD, B-Section V-Belt (Driver)	1
Quick-Disconnect Bushing (SH, Standard Keyway, 7/8" Bore)(Driver)	1
Bushing-Bore Pulley, B-Section V-Belt (Driven)	1
Quick-Disconnect Bushing (SDS, Standard Keyway, 1.5" Bore)	1
B-Section V-Belt (48')	2
Oversized Steel Machine Key Stock (Zinc-Plated)	2
1045 Carbon Steel, 1-1/2" Diameter, 12" Long Keyed Rotary Shaft	1
SKF Y-Bearing Units	2
Steel Unthreaded Spacer, 1.5" OD x .75" ID x 1" Lg.	1

Acquisition Status



In Stock

In Transit

To Be Purchased

System Type



Drivetrain

Fastener

Frame



Misc.

Power



Steering

Suspension

		▼ Sum of Quantity
Grade 8 Steel, 1/4"-20 Thread Size, 1-3/8" Long		25
Flanged, 1/4"-20 Thread Size, 5/8" Long		50

Acquisition Status 	System Type 
<input checked="" type="checkbox"/> In Stock	<input type="checkbox"/> Drivetrain
<input type="checkbox"/> To Be Purchased	<input checked="" type="checkbox"/> Fastener
	<input type="checkbox"/> Frame
	<input type="checkbox"/> Misc.
	<input type="checkbox"/> Power
	<input type="checkbox"/> Steering
	<input type="checkbox"/> Suspension

		▼ Sum of Quantity
Aluminum 6061 1" Square Tubing (20' Length)		9
Driver Seat		1

Acquisition Status 	System Type 
<input checked="" type="checkbox"/> In Stock	<input type="checkbox"/> Drivetrain
<input type="checkbox"/> To Be Purchased	<input type="checkbox"/> Fastener
	<input checked="" type="checkbox"/> Frame
	<input type="checkbox"/> Misc.
	<input type="checkbox"/> Power
	<input type="checkbox"/> Steering
	<input type="checkbox"/> Suspension

	▼ Sum of Quantity
48V 20AH LiFePO4 Battery	1
48V 50A Battery Management System	1
Solar Module (53-3/4" X 29-5/32")	1
T5500 Lithium Battery Case	1
VeriBest 48V 4A Lithium Battery Charger	1
Zip Ties	10
MorningStar TS-45 Charge Controller	1

Acquisition Status



In Stock

In Transit

System Type



Drivetrain

Fastener

Frame

Misc.

Power

Steering

Suspension

	▼ Sum of Quantity
Wheel (Steering)	1
Rack (Gearbox)	1
Universal Joint	1
Tie Rods	2
Bushing (Steering)	1
Bushing Collar (Steering)	1
Column (Steering)	1

Acquisition Status

In Stock

System Type



Drivetrain

Fastener

Frame



Misc.

Power

Steering

Suspension

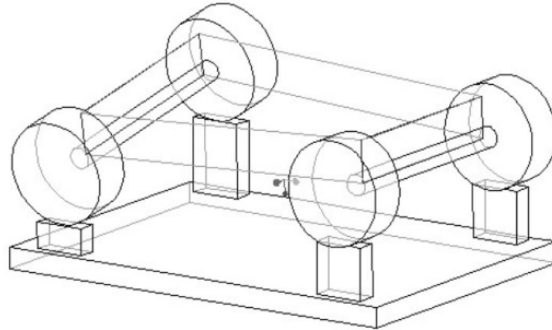
▼ Sum of Quantity	
Tires & Rims	4
Hex Head Shoulder Bolt, 3/8"-16 Thread	16

Acquisition Status 	System Type 
<input checked="" type="checkbox"/> In Stock	<input type="checkbox"/> Drivetrain
<input type="checkbox"/> To Be Purchased	<input type="checkbox"/> Fastener
	<input type="checkbox"/> Frame
	<input type="checkbox"/> Misc.
	<input type="checkbox"/> Power
	<input type="checkbox"/> Steering
	<input checked="" type="checkbox"/> Suspension

Appendix C: Frame Design

LONGITUDINAL TORSION

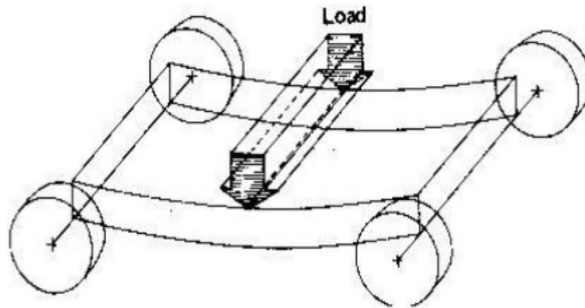
Longitudinal torsion results from a difference in the normal force applied in the tires of the vehicle when cornering, or passing through obstacles in the road. For this case, the chassis could be imagined as a torsional spring that connects the front and rear suspension of the vehicle. The resistance of the chassis to longitudinal torsion is called torsional rigidity, and it is determinant factor of chassis performance as it will be described later.



Longitudinal torsion deformation [28]

VERTICAL BENDING

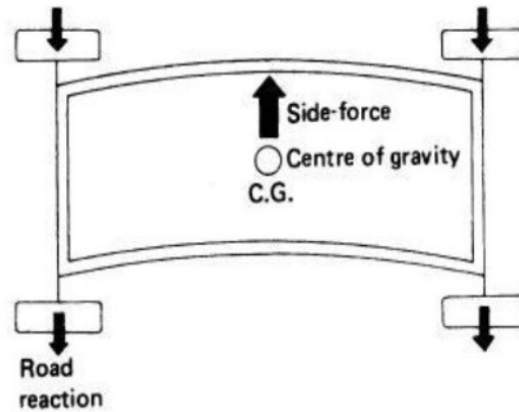
Vertical bending results from loads applied in the vertical plane of the chassis. For example, Weight of driver, chassis, and engine. It is important to note that vertical accelerations may change the intensity of those loads.



Vertical Bending Deformation [28]

LATERAL BENDING

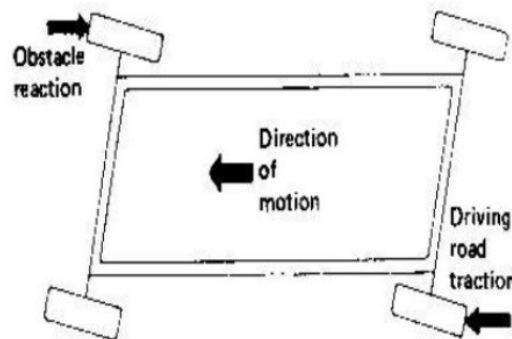
Loads that produce lateral bending, can be originated due to many reasons. For example, lateral loads produced by wind or centrifugal forces when cornering.



Lateral Bending Deformation [28]

LOZENGING HORIZONTAL

Lozenging horizontal deformation happens when loads are applied in opposite tires with opposite directions. This type of load can happen due to small variations on the road.



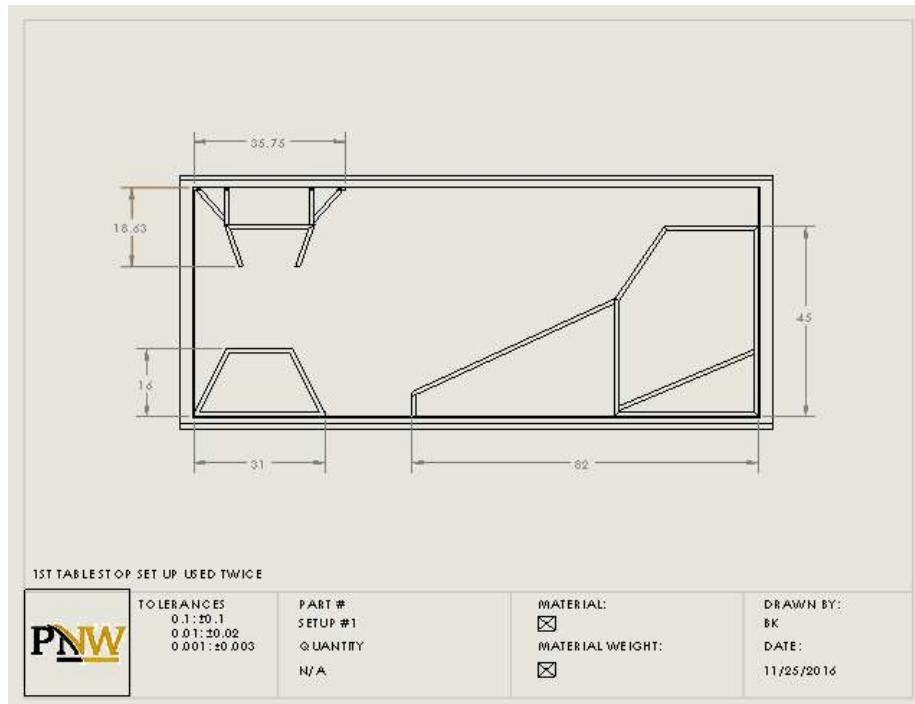
Lozenging horizontal deformation [28]

Appendix D: Bill of Materials

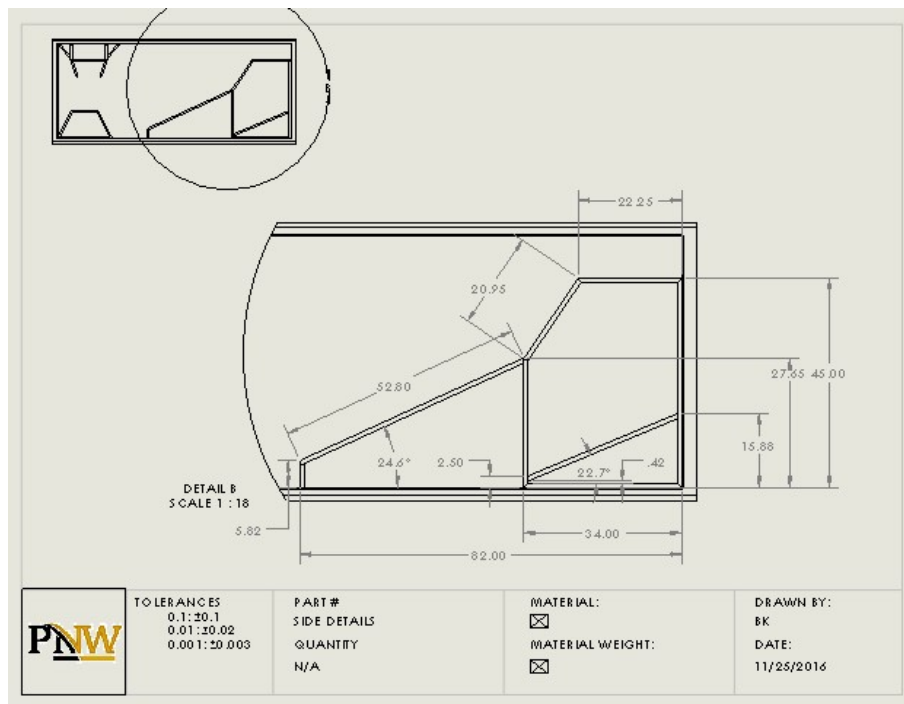
Part #	Quantity (#)	Length of Member (in)	Length of Member Type (in)
1	2	27.65	55.3
2	2	34	68
3	2	45	90
4	2	22.25	44.5
5	2	20.95	41.9
6	10	34	340
7	1	39.37	39.37
8	2	35.1	70.2
9	2	14.27	28.54
10	2	12.53	25.06
11	1	31	31
12	2	38.98	77.96
14	2	16.77	33.54
15	1	15.62	15.62
16	2	11.34	22.68
17	2	17.49	34.98
19	2	15.97	31.94
20	2	53.14	106.28
21	1	5.18	5.18
22	1	36	36
23	1	5.18	5.18
24	2	19.73	39.46
25	2	12.28	24.56
26	2	22.24	44.48
28	1	29	29
29	1	14	14
31	1	31.53	31.53
32	2	18.83	37.66
33	2	12	24
34	4	10.94	43.76
35	2	21.41	42.82
36	2	11	22
37	2	19.4	38.8
38	2	25.66	51.32
40	1	43.35	43.35
42	1	36.48	36.48
43	1	33.97	33.97
44	2	18.22	36.44
47	2	8.63	17.26
50	4	18.08	72.32
51	2	16.16	32.32
52	2	3.15	6.3
53	2	21.27	42.54
54	2	10.49	20.98
56	2	27.47	54.94
Total Length of Tubing (ft)			189.21
Total Amount of Tubing At ArrowPin (ft)			216
Amount Needed (ft)			-26.79

Appendix E: Frame Fabrication Drawings By Setup

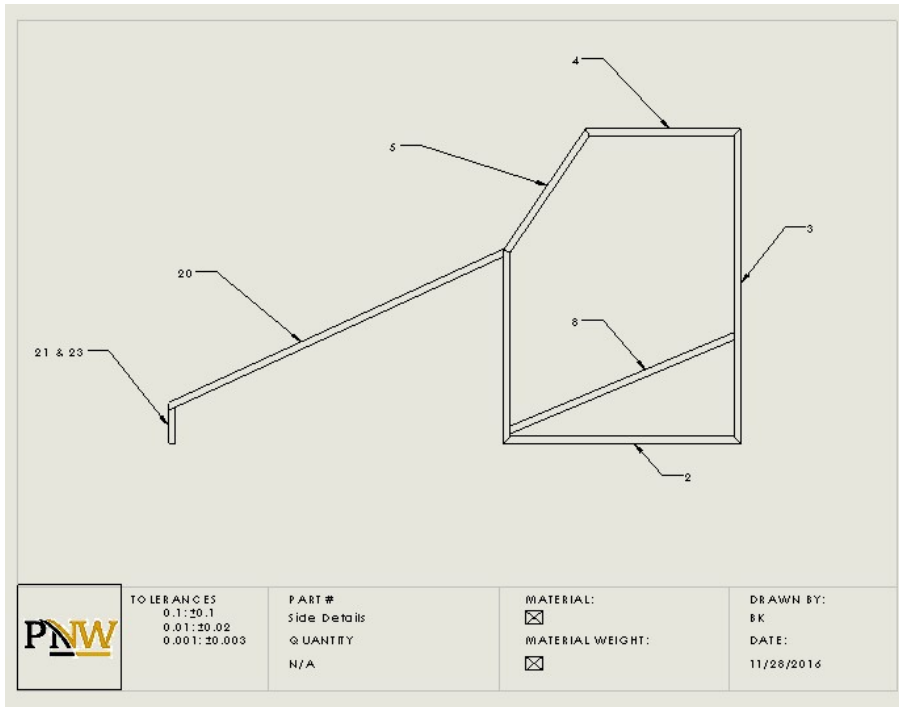
Setup #1: Suspension Trapezoids and Side Sections (2 Rounds of Welding)



Overall Table Setup 1

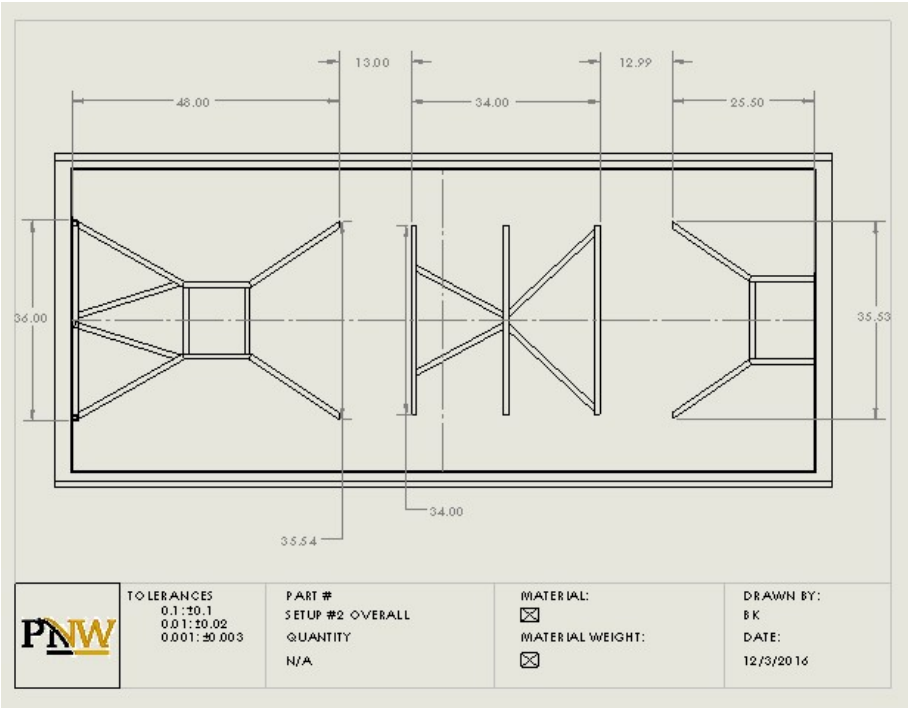


Dimensioned Table Stop Drawing.

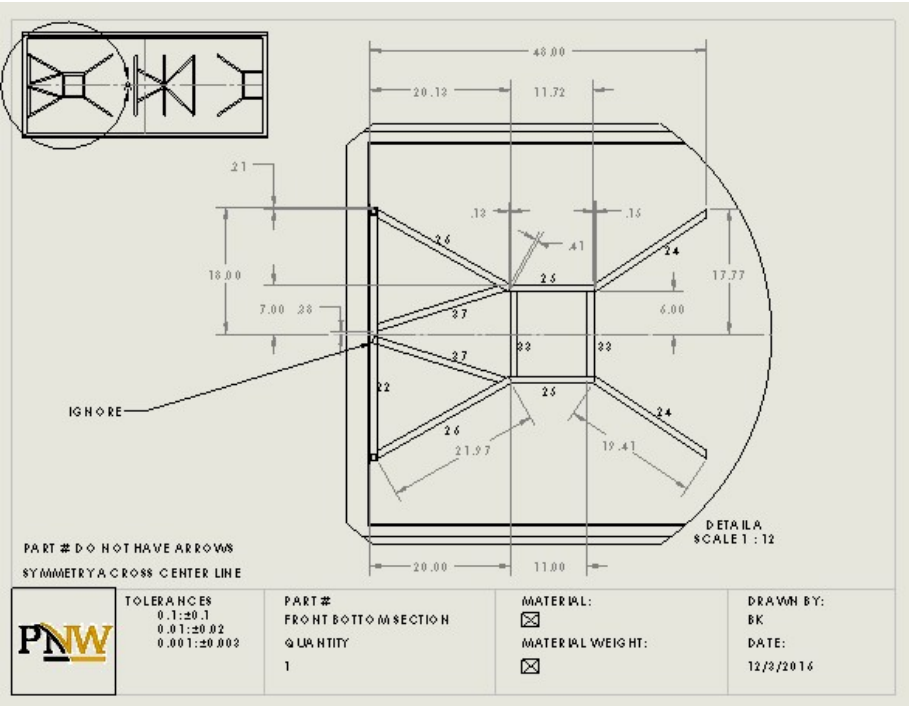


Member Description Drawing.

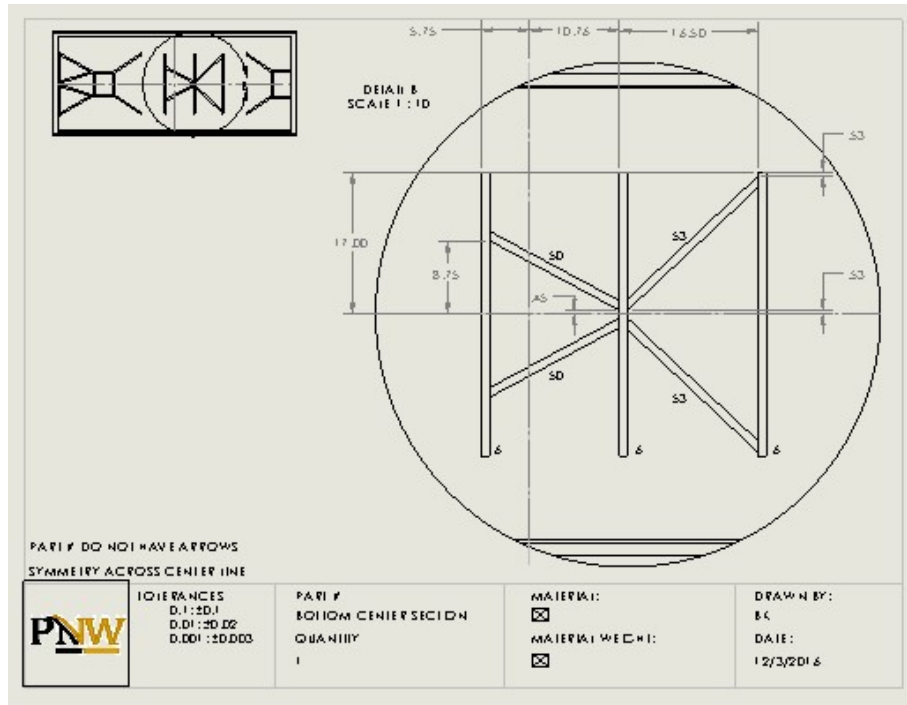
Setup #2: Bottom Sections



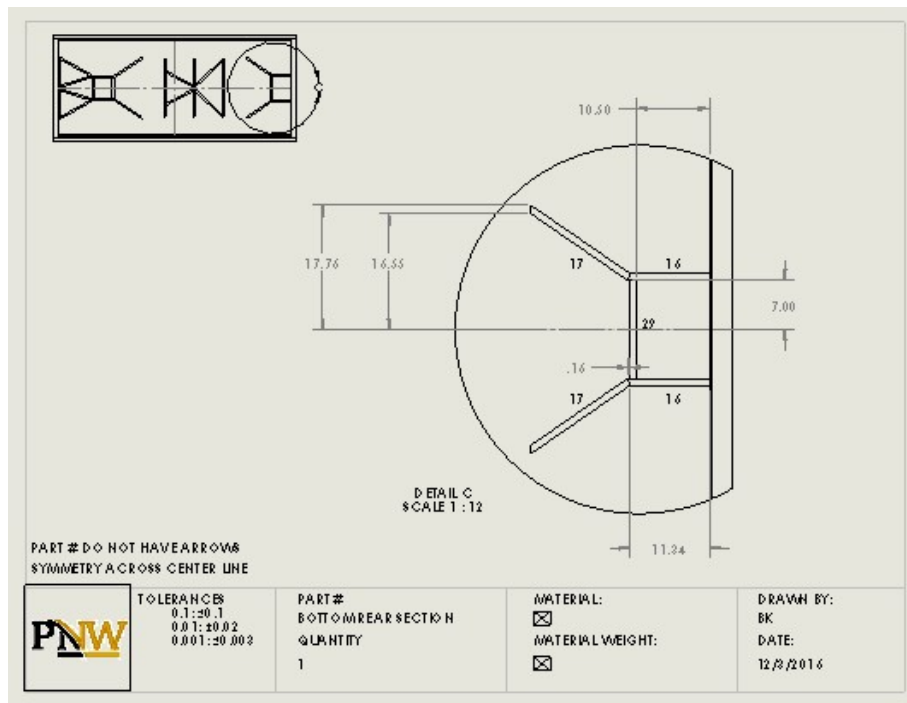
Overall Table Setup 2



Detail Dimension of Front Section

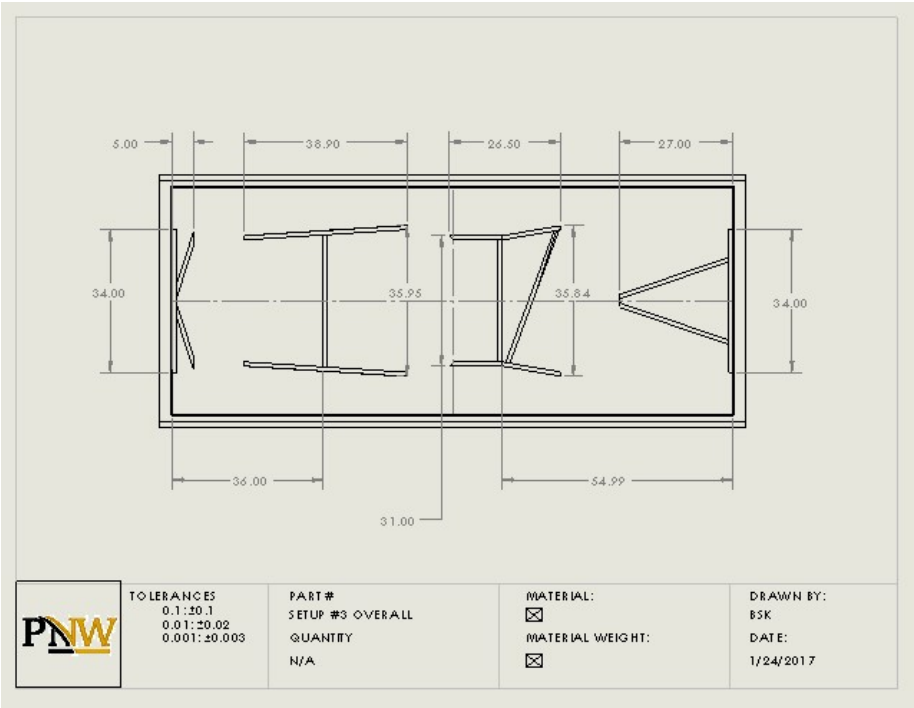


Detailed Dimension of Mid Section

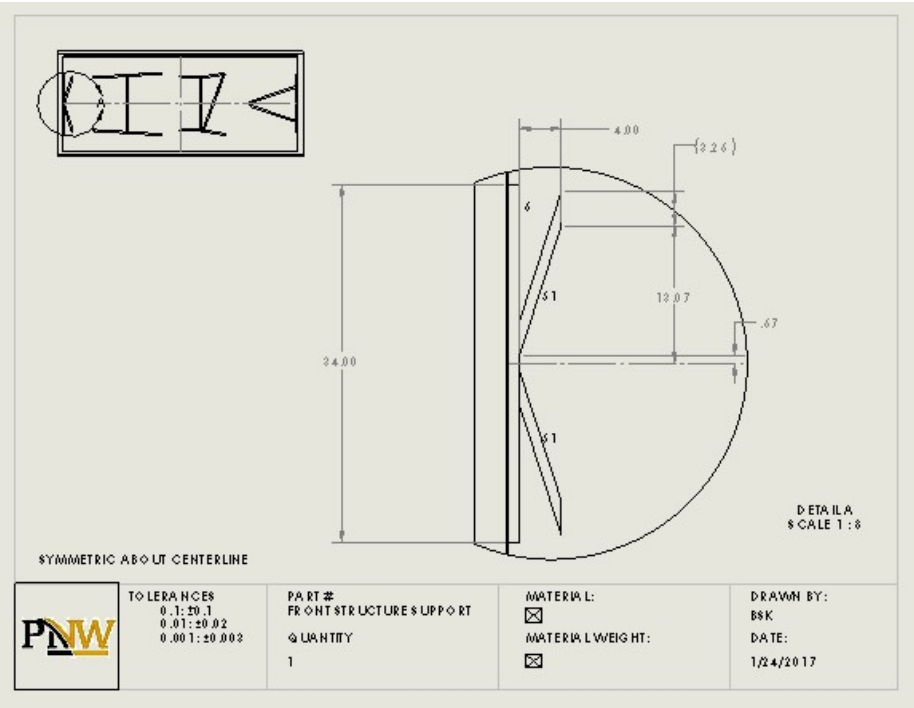


Detailed Dimension of Rear Section

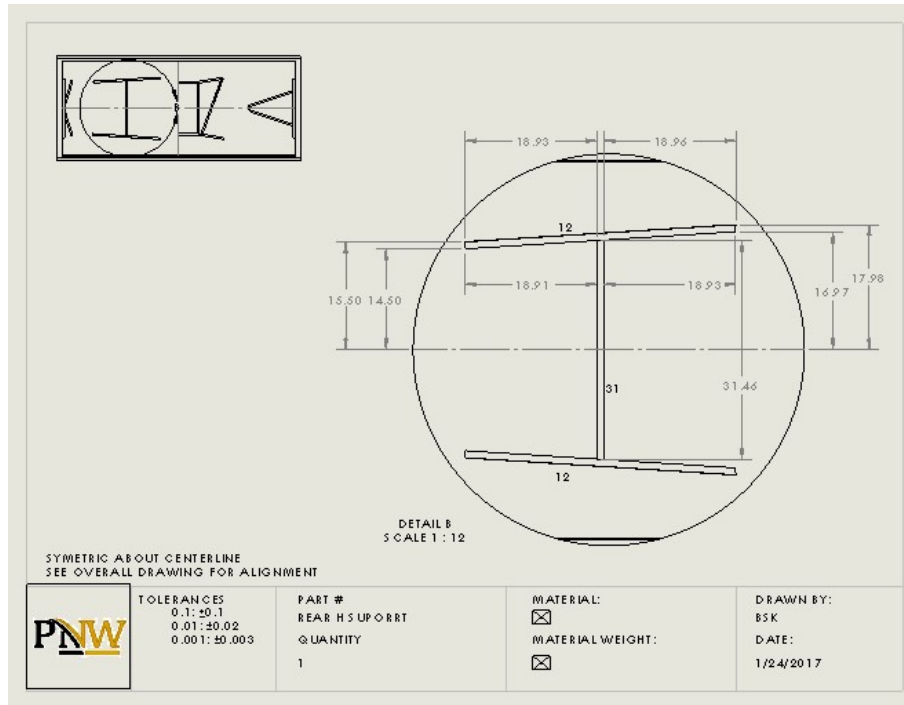
Setup #3: Front Planar, Rear “H”, Rear Mid Suspension, Steering Mounting



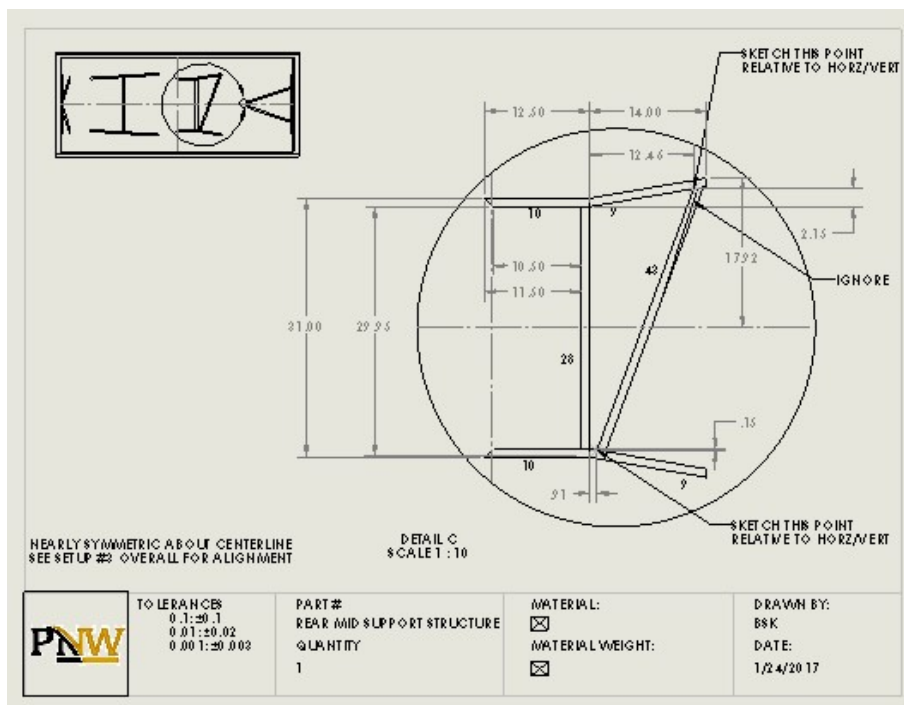
Overall Table Setup 3



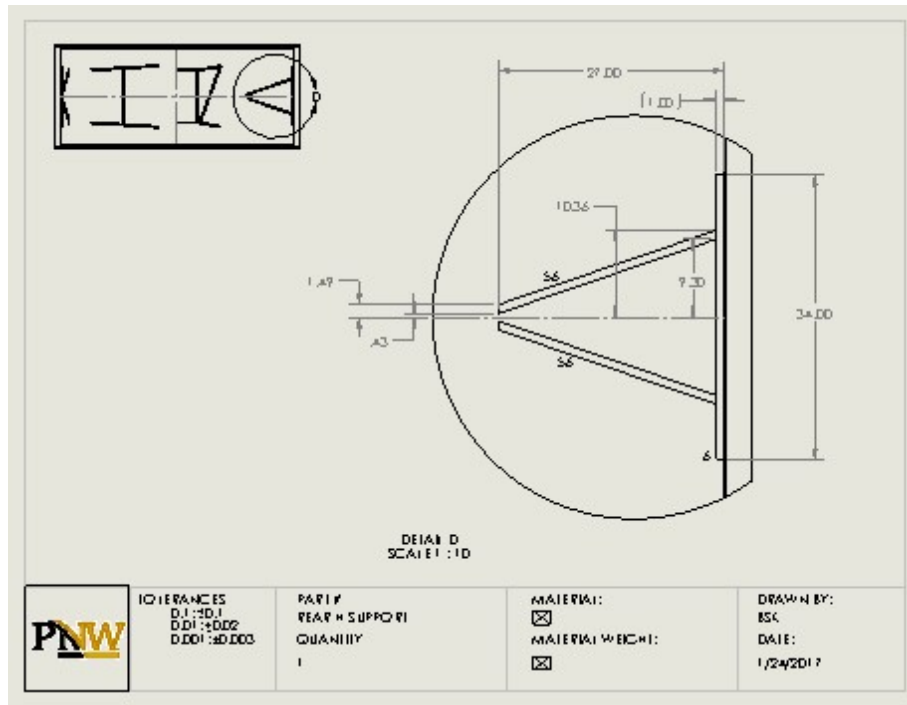
Detailed Dimension of Front Planar Section



Dimension of "H" Support

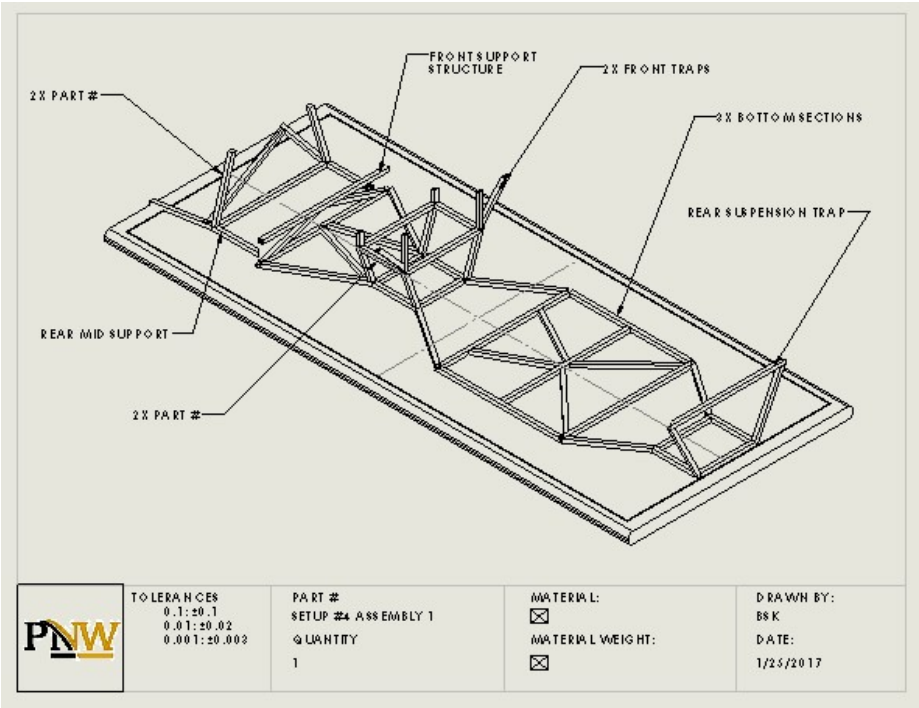


Dimension of Rear Mid Suspension Support

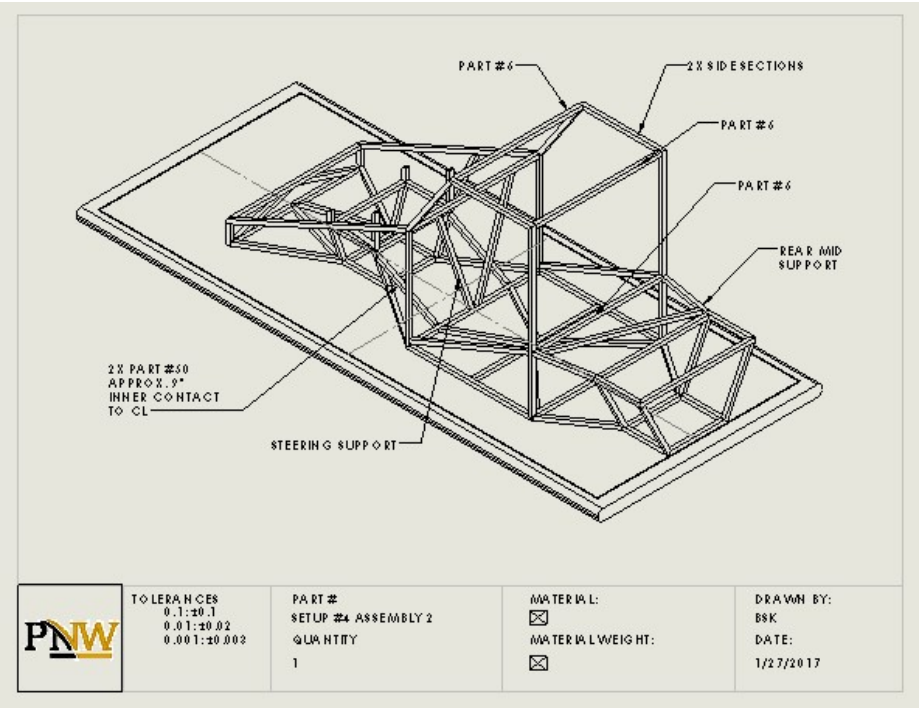


Dimension of Steering Mounting Structure

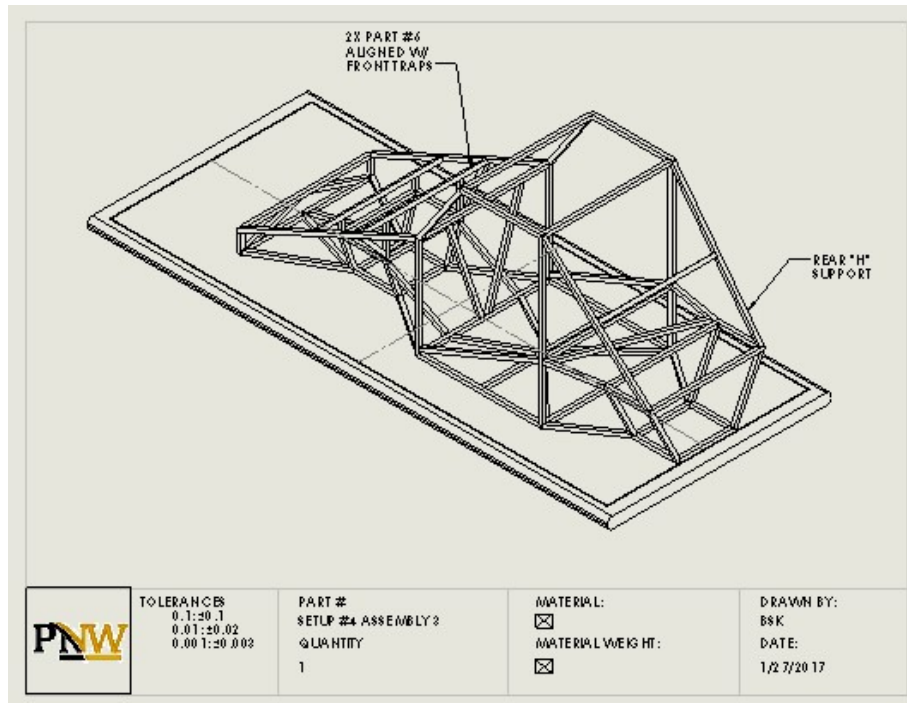
Setup #4: Section Mounting and Finalization



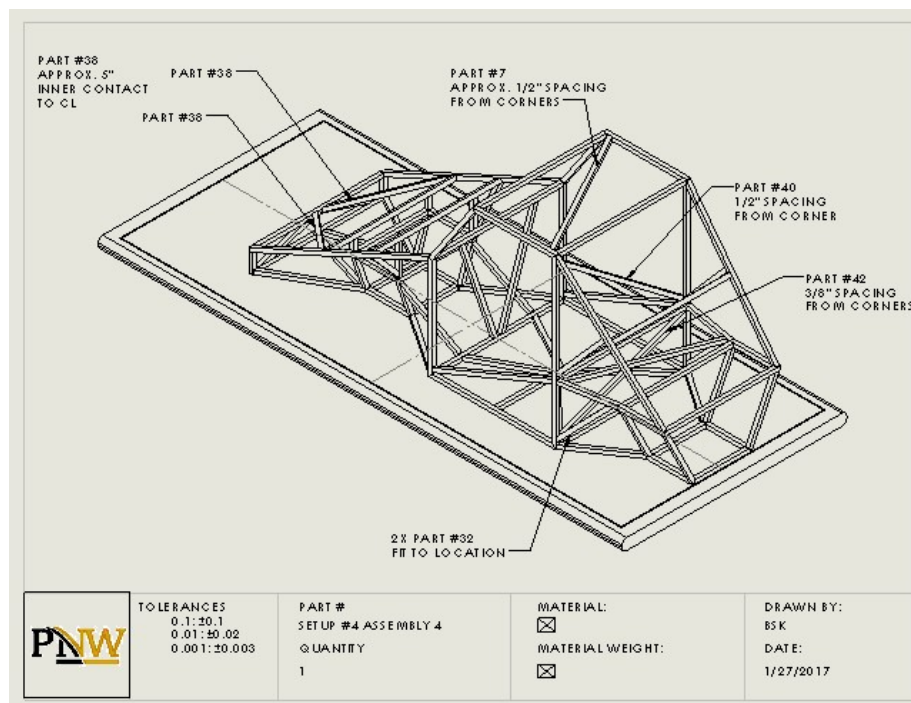
Assembly 1



Assembly 2

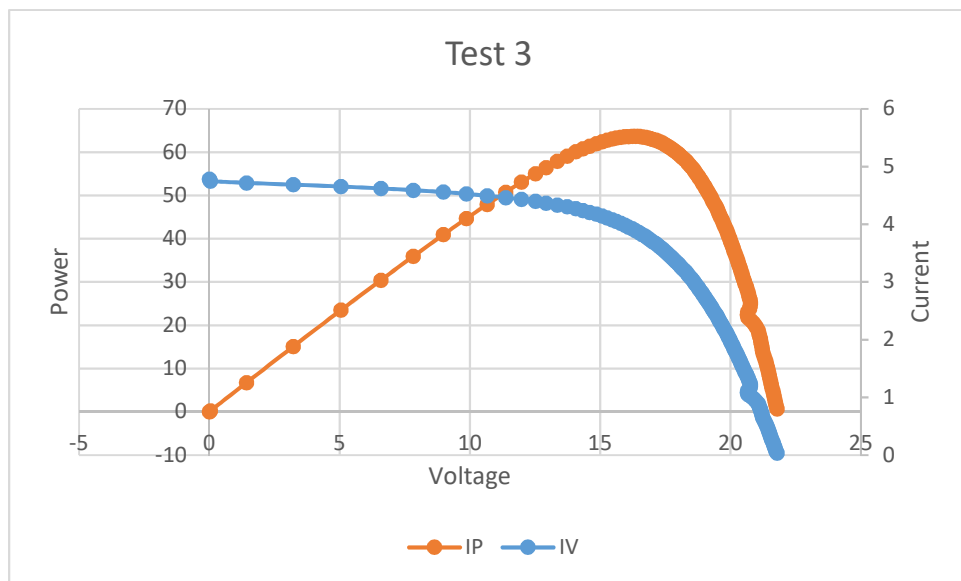
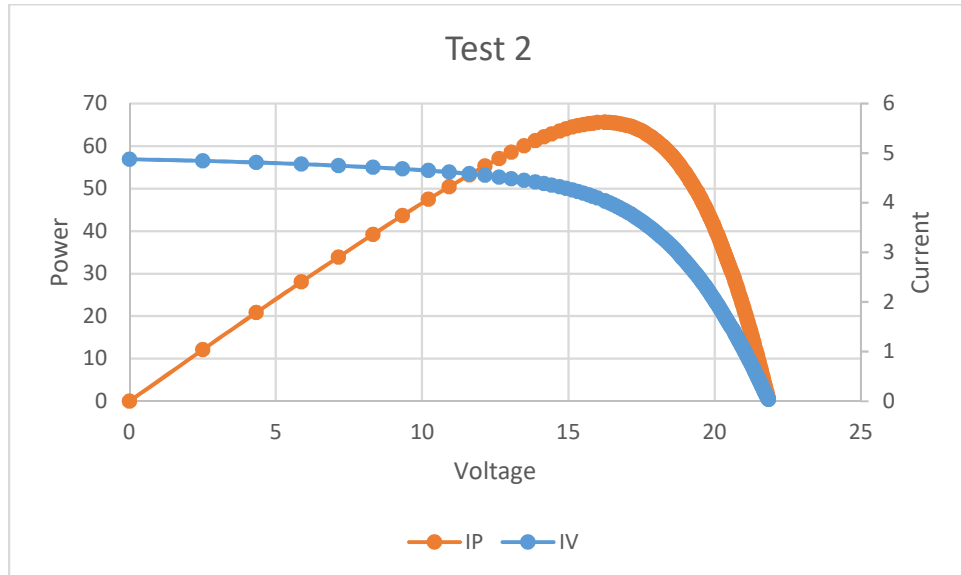


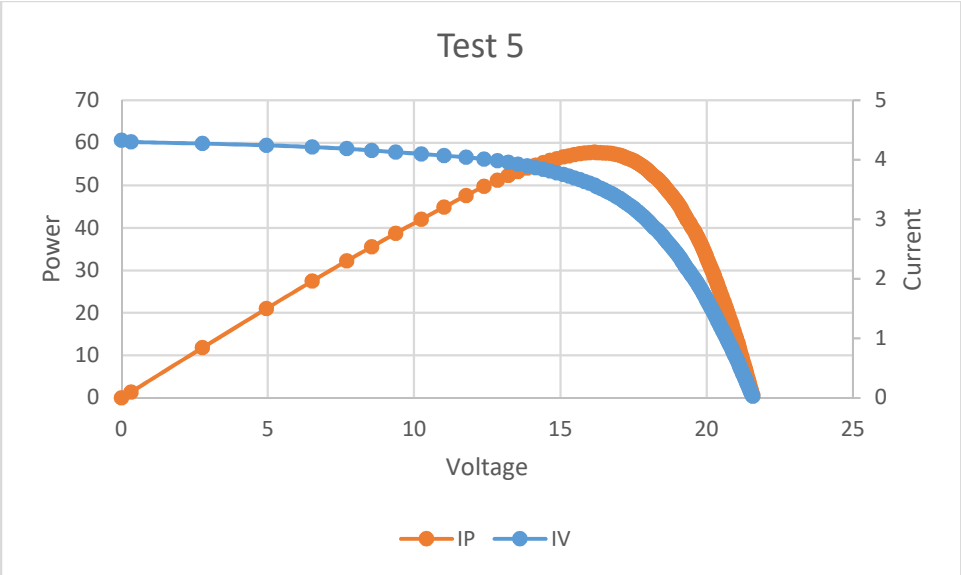
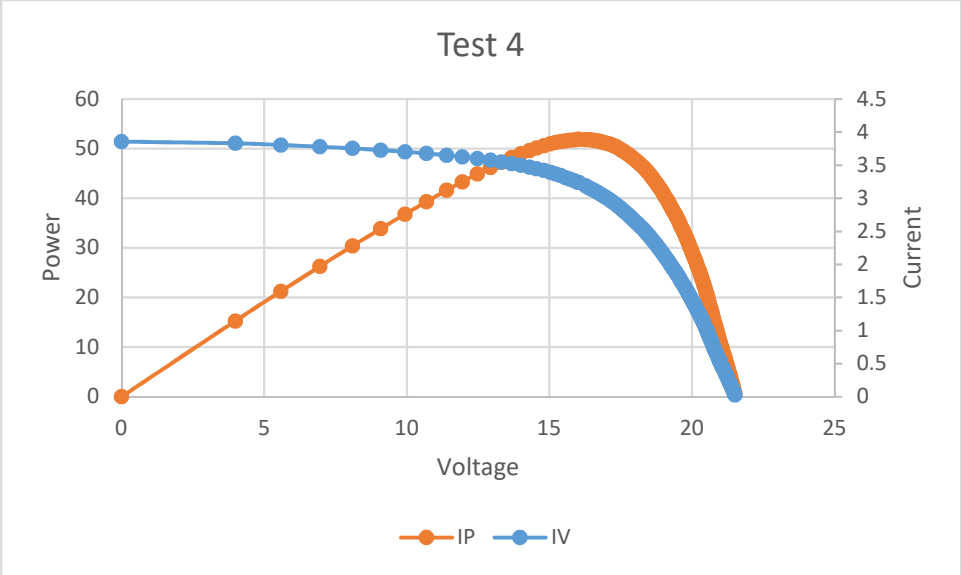
Assembly 3



Assembly 4 (Completed Frame)

Appendix F: Solar Panel Data and Graphs

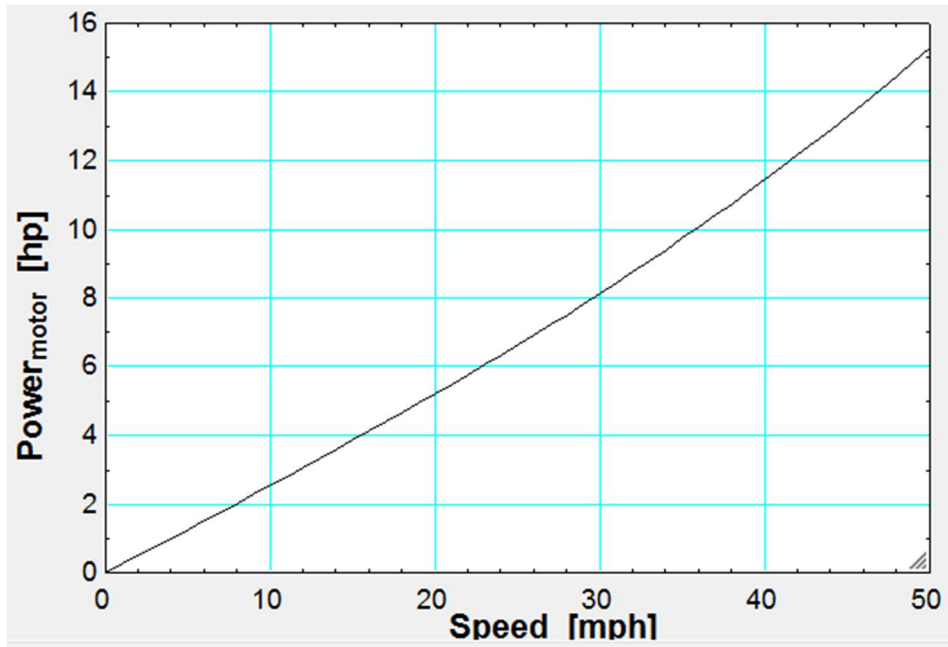




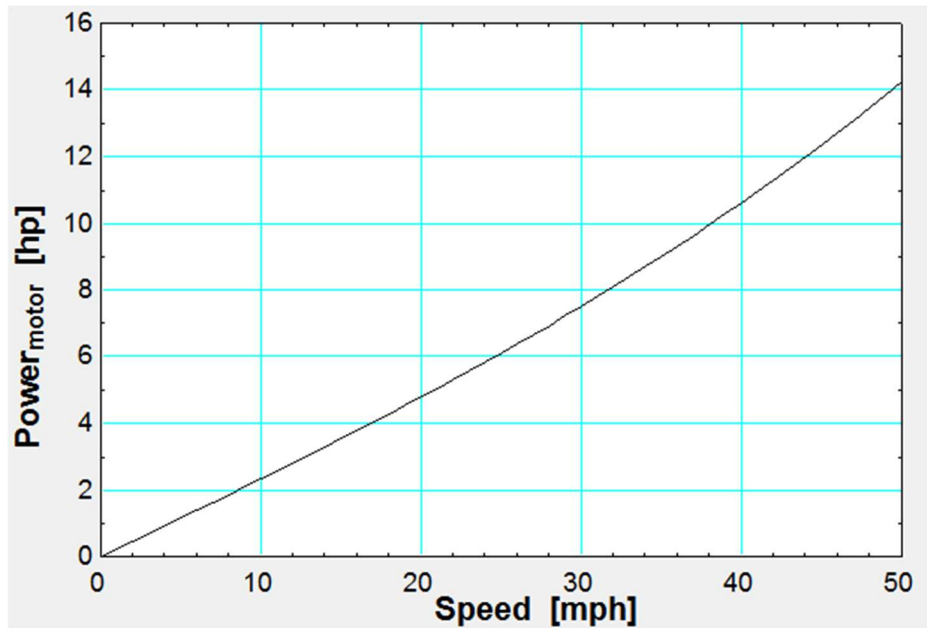
Appendix G: Motor Sizing Calculations and Data

EES Equations Window	
W=700 [lbs]	"Weight of Vehicle"
R=.75 [ft]	"Tire Radius"
A_f=18.191 [ft^2]	"Frontal Area"
a=0 [mph/s]	"Acceleration"
rho=0.075169 [lb/ft^3]	"Density of Air"
theta=0 [deg]	"Angle of Inclination"
"Speed=10"	
GR=5	"Overall Gear Ratio"
eta=.85	
C_r=0.018	"Rolling Coef"
C_i=1.06	"Inertia Coef"
C_d=0.15	"Drag Coef"
F_r=W*C_r*cos(theta)	"Rolling Resistance"
F_a=C_i*W*a/21.95	"Acceleration Resistance"
F_c=W*sin(theta)	"Climbing Resistance"
F_d=rho/2*C_d*A_f*(Speed*1.467)^2/32.2	"Drag Force"
RPM_wheels=Speed*1.467/2/3.14/.75*60	
F_tot=F_r+F_a+F_c+F_d	
Torque_wheels=F_tot*R	
Torque_motor=Torque_wheels/GR	
RPM_motor=RPM_wheels*GR	
Power_motor=Torque_motor*RPM_motor/5252/eta	

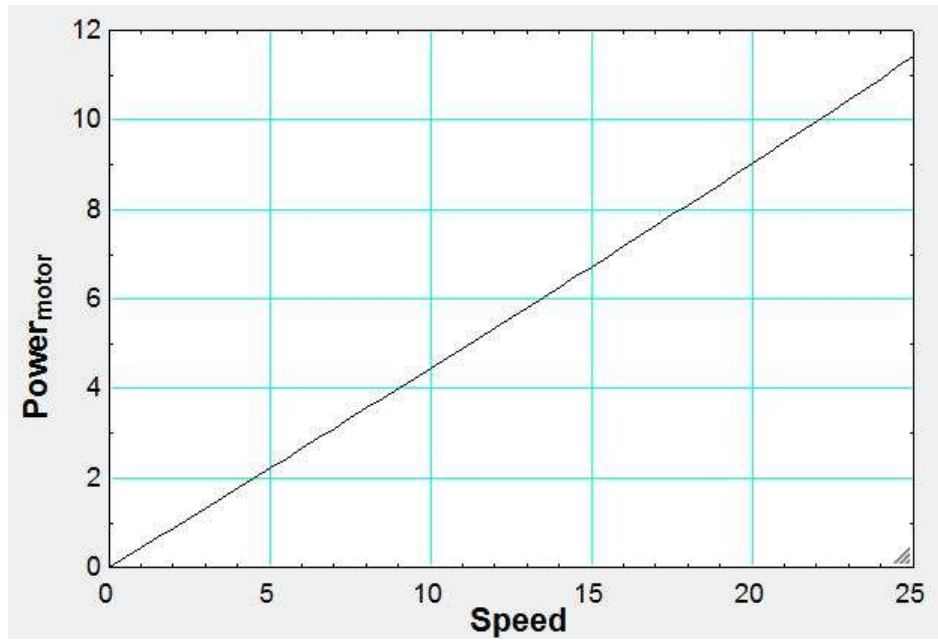
EES Code for parametric analysis for motor sizing.



Power Required vs. Speed (Level Ground with 2mph/s Acceleration).



Power Required vs. Speed (5° Incline with no Acceleration)



Power Required vs. Speed (5® Incline with 2mph/s Acceleration)